UNIVERSITY OF TURKU
Faculty of Science

The effect of macrophages on the hormone-releasing cells in mouse pituitary

Elina Laine

Physiology & Genetics
Master's thesis
Credits: 30

Supervisors:
Heli Jokela
Tiina Henttinen

5.5.2022
Turku

Master's thesis

Subject: Physiology and Genetics
Author: Elina Laine
Title: The effect of macrophages on the hormone-releasing cells in mouse pituitary
Supervisors: Heli Jokela, Tiina Henttinen
Number of pages: 49 pages + 6 appendixes
Date: 5.5.2022

At the base of the brain is located the pituitary gland which secretes hormones to the bloodstream. Among other cells, the pituitary is resided by macrophages which take part in the immune system by phagocyting pathogens. I studied if macrophages have an impact on the hormone-releasing cells in mouse anterior pituitary and if they share the same intratissue localization. RNAscope® assay was used to evaluate macrophage-specific gene expression in the pituitary of wild-type mice. Then, both hormone-releasing cells and macrophages were studied by immunofluorescence staining. The number of active hormone-releasing cells secreting growth hormone, luteinizing hormone, prolactin and thyroid-stimulating hormone were compared between wild-type and Plvap$^{-/-}$ mice. The knock-out model lacks macrophages derived from the fetal liver. Lastly, pituitary tissue sections from wild-type mice and CCR2$^{-/-}$ and Nur77$^{-/-}$ mice were haematoxylin and eosin stained for histological comparison. Murine CCR2 is involved in macrophage recruitment and Nur77$^{-/-}$ mice do not have Ly6C^{low} monocytes.

The RNAscope® assay appeared not to be the best method to study the targeted genes and so, different macrophage populations could not be identified. Another method might be found to get clear results from the macrophage populations in question. Macrophages could not be detected in the immunofluorescence experiment together with the hormonal cells. However, the results showed that Plvap$^{-/-}$ have less cells secreting growth hormone and luteinizing hormone than wild-type mice, while the number of the other studied hormonal cells were not significantly different between the mouse strains. Earlier hormonal measurements have resulted in low prolactin levels in Plvap$^{-/-}$ pituitary so it is interesting that the number of hormonal cells is not lower in the knock-out pituitaries. Also, both macrophages and the hormone-releasing cells would be beneficial to get detected at the same time. The histological comparison did not show any differences in the pituitary sections of CCR2 and Nur77 knock-outs and wild-type mice. Changes in these two knock-out models do not seem to affect the colonization and the number of the hormone-releasing cells in the pituitary gland. Overall, macrophages originating from the fetal liver seem to affect the secretory cells of growth hormone and luteinizing hormone while the monocyte-derived macrophages do not. More studies focusing on this phenomenon are needed.

Keywords: pituitary gland, anterior lobe, macrophages, hormone-releasing cells, RNAscope, immunofluorescence, haematoxylin and eosin staining, knock-out, mouse, Plvap, CCR2, Nur77, growth hormone, prolactin, luteinizing hormone, thyroid-stimulating hormone

Contents

1 INTRODUCTION

The brain controls all the functions of the body by taking and processing information from outside and inside the body and transporting responding signals to tissues. The brain is composed of different sections that control a specific type of information and have distinct roles. The hypothalamus is one small part of the brain formed by various nuclei and nerve fibers. Its location is at the base part of the brain and it is connected to the pituitary gland, which secretes specific hormones into the bloodstream. The secretion of those hormones is regulated by the hypothalamus; thus, the pituitary gland serves as a link between the nervous system and the endocrine system.

The brain, among other tissues, is colonized with specialized cells called macrophages. These cells help the body fight against pathogens and other harmful organisms. Macrophages have other purposes as well since they are involved in tissue development and maintaining a stable internal state in the body. Depending on the target tissue, macrophage populations have different names and functions.

There are various ways to study the body depending on the tissue and target components. To get information about localization of the cells, like macrophages and hormone-releasing cells or structures like the lobes of the pituitary gland, staining methods come in handy. Stains can adhere to certain cell components or the entire cell. Staining can target DNA, proteins, lipids, carbohydrates etc. Many stains can be imaged with simple brightfield microscopes but some staining methods use fluorophores as stains and can be detected using a fluorescent microscope or a confocal microscope.

1.1 Pituitary

Pituitary is a small endocrine gland located at the base of the brain. Human pituitary is connected to the hypothalamus by an infundibular stalk which is a tube-like structure. The pituitary has three different lobes (Figure 1), which are the posterior lobe (pars nervosa), the intermediate lobe (pars intermedia) and the anterior lobe (pars distalis). The posterior lobe receives fibers from large neurons in the hypothalamus and it works as a connecting part to the brain. The posterior and anterior lobes are separated by the intermediate lobe. The anterior and posterior lobes take up most of the gland while the intermediate lobe is narrow and only notably visible in some species, for example in rodents. The lobes are embryologically, functionally, and morphologically distinct from each other.

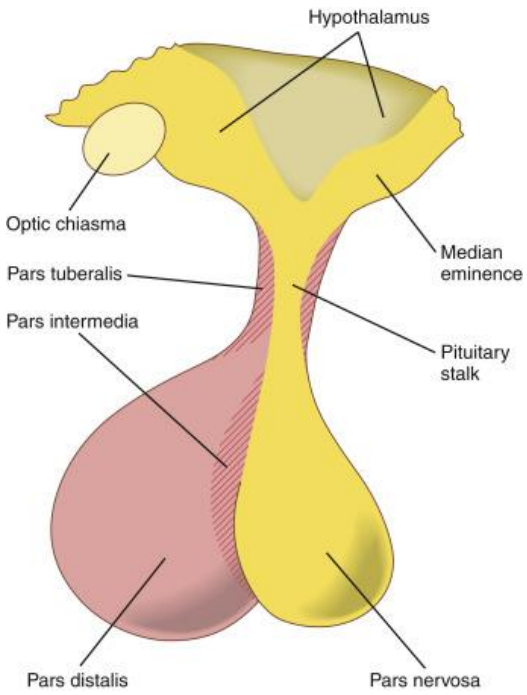

Figure 1. Overview of the human pituitary, its three lobes and how it is connected to the hypothalamus (Jones & Lopez 2015).

The anterior lobe is the secretory lobe of the pituitary and also the largest lobe. It has many hormone-releasing endocrine cells and glial-like non-endocrine cells releasing growth factors or inflammatory cytokines. It also contains nests and cords of these secretory cells. Both the anterior lobe and the intermediate lobe have their embryological origin in Rathke's pouch, the anterior lobe originating from the oral cavity. The intermediate lobe is avascular and has cysts that are either empty or filled with colloid. These cysts are lined by flattened epithelium. Individual cells are cuboidal or

columnar and lie on a stroma, which is slightly fibrous. The third lobe, the posterior lobe, has its origin in the neural ectoderm at the floor of the forebrain. The posterior lobe is mostly constructed of nonmyelinated axons of hypothalamic neurons that hold neurosecretory peptides. It also has non-neuronal cells, glia, and modified glia which are called pituicytes. Oxytocin and vasopressin are secreted from the posterior lobe. The shape of the cells in the posterior lobe is elongated with variably elongated nuclei. (Hagan et al. 2012.)

There are many differences between the human and mouse pituitary. The human pituitary is prominently lobulated and the mouse pituitary has more homogenous appearance (Hagan et al. 2012). The shape of the gland is notably different as well. The human pituitary has a round-like figure while the mouse pituitary is more elongated (Figure 2). In the human pituitary cells are arranged in rosettes and clusters, also age-related mineralization can happen.

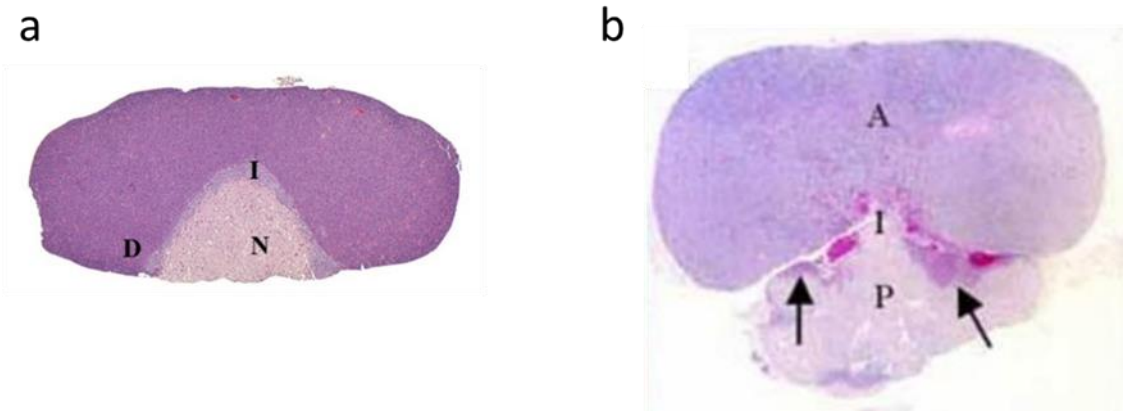

Figure 2. (a) Horizontal section of a mouse pituitary gland and its lobes: the posterior lobe (N), the intermediate lobe (I) and the anterior lobe (D); Maronpot & Brix (2014). (b) Horizontal section of a human pituitary gland and its lobes: the posterior lobe (P), the intermediate lobe (I) and the anterior lobe (A); Asa (2007). Sections are not in scale with each other.

From the tree lobes, the intermediate one is a remnant in the human pituitary. It is relatively larger in mice and much better developed. The intermediate lobe in mice is separated from the anterior lobe by a cuboidal epithelium-lined cleft. The cytoplasm is foamy and nuclei have an ovoid shape. The cells are slightly larger than the cells in the anterior lobe. Even though some anterior lobe cells can secrete adrenocorticotropic hormone (ACTH) and melanocyte-stimulating hormone (MSH), most of the secretion of

those hormones is located in the intermediate lobe. This is also a feature of mouse intermediate lobe that differs from the human pituitary. (Hagan et al. 2012.)

In mouse, the pituitary gland rests in the center of the skull base locked between semilunar ganglia (Figure 3). These ganglia keep the pituitary in place but the gland is also rigidly attached to the skull by a fibrous membrane. The pituitary is oriented so that the posterior lobe is facing the brain surface. The difference in the human pituitary's location is that it is within a hollow area of the sphenoid bone, called the sella turcica, behind the nose bridge. In orientational difference, the human posterior lobe is facing the back of the scull as its name suggests. The posterior lobe is also relatively smaller in the mouse pituitary. Female mice have a larger pituitary compared to male mice.

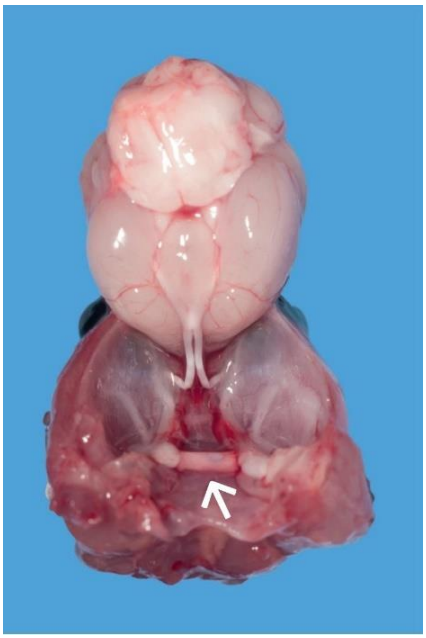

Figure 3. Gross view of the adult mouse brain *in situ* (Hagan et al. 2012, modified). The white arrow points at the pituitary which can be seen at the bottom of the scull when the brain is removed. Round-like, pale structure on the surface of the pituitary is the posterior lobe.

Even though the pituitary is small, it is a vital gland. Its hormones regulate several functional aspects of our body, from growth to metabolism. The anterior lobe of the pituitary secretes many hormones that affect different parts of the body in specific ways. The lobe consists of cell clusters that produce six different hormones. Corticotropic cells produce adrenocorticotropic hormone (ACTH), thyrotropic cells produce thyroid-stimulating hormone (TSH), somatotropic cells produce growth hormone (GH), gonadotropic cells produce both follicle-stimulating hormone (FSH) and luteinizing

hormone (LH), and lactotrophic cells produce prolactin (PRL). The hormone-releasing cells are under the regulation of the hypothalamus. The hypothalamus produces the corticotrophin-releasing hormone, growth hormone-releasing hormone, gonadotrophin-releasing hormone, thyrotrophin-releasing hormone, somatostatin and dopamine. Somatostatin inhibits the production and secretion of GH and TSH, while dopamine inhibits the PRL production and secretion. Hypothalamic hormones are secreted to the anterior lobe by capillaries within the infundibular stalk. This hypophyseal portal system, which at least humans have, allows transportation without the hormones first entering the systemic circulation. Superior hypophyseal artery, which transports blood to the hypothalamus, is the origin of the system. Hormones from the hypothalamus reach the anterior lobe of the pituitary by first going through a primary capillary plexus to the portal veins. Released hormones from the anterior lobe enter a secondary capillary plexus from where they drain into the bloodstream.

1.2 Macrophages and their functions

Macrophages are specialized cells that are part of innate immunity. They discard harmful organisms by phagocytosis, but they also initiate inflammation and present antigens. In addition, macrophages are involved in regulating tissue homeostasis and development. Some of the macrophages are permanently located within different tissues. Depending on the localization in the body, these tissue-resident macrophage populations can have different names, and their functions are tissue-specific. For example, tissue-specific macrophages found in the liver are called Kupffer cells, and macrophages in the central nervous system are called microglia. Tissue-specific behaviour occurs since macrophages can react to their environmental conditions. Among Kupffer cells and microglia, the tissues are colonized with other types of macrophages as well.

Some of the macrophages differentiate from monocytes, which are a type of leukocyte, circulating in the bloodstream. Macrophages are larger than monocytes and they have more intracellular organelles. They are mononuclear myeloid cells that can migrate and respond to their environment. The most known feature of macrophages is that they phagocyte pathogens and apoptotic cells and destroy them with oxygen-dependent free radicals or oxygen-independent hydrolases. Macrophages can start an inflammatory process when certain microbial products are activating them. Inflammatory process means presenting antigens to T cells, which are one of two primary types of lymphocytes,

with the help of major histocompatibility complex (MHC) protein and secreting cytokines. These cytokines also activate T cells with the aid of effective antigen presentation. This way macrophages associate innate and adaptive immunity. In addition, macrophages secrete chemokines, complement components, lipids, and growth factors.

1.2.1 Origin

There are tissue-specific macrophages but also monocyte-derived macrophages, which can differentiate into tissue-specific macrophages. It was thought that tissue-specific macrophages originate from the hematopoietic stem cells in the bone marrow. However, more recent studies have shown that tissue-specific macrophages differentiate from erythro-myeloid progenitors (EMP) in the fetal yolk sac and this happens without monocyte interphase (Hoeffel & Ginhoux 2018). These early stem cells differentiate into primary macrophages which mainly form the microglia population in the brain. Other EMP stem cells travel from the yolk sac to the fetal liver, differentiate into monocytes and then into macrophages. Two distinct transcription factor sets guide to the development of macrophages (T'Jonck et al. 2018). Lineage-determining transcription factors establish a core macrophage program during the pre-macrophage stage. The program is influenced by specific signals from the tissue, while it is also refined by signal-dependent transcription factors. The influence and refinement allow the macrophages to have tissue-specific functions. In adults, hematopoietic stem cells in bone marrow develop monocytes which can differentiate into macrophages in tissues (Hoeffel & Ginhoux 2018).

Some tissue-specific macrophages can self-renew but those that cannot are replaced by differentiated monocytes. Self-renewal and macrophage-replacement depend on the self-renewal capacity of the tissue macrophages and accessibility to the blood of the particular organ (Ginhoux & Guilliams 2016). For example, the skin dermis and intestine get new macrophages through monocyte migration and differentiation. Tissues with low access to blood, such as the epidermis, the lungs, and the brain, depend on self-renewal of the resident macrophage populations. When the number of tissue-specific macrophages drops drastically, replication of resident macrophages increases, as well as recruitment of monocytes that differentiate into macrophages (Guilliams & Scott 2017). Those recently differentiated macrophages will be maintained through self-renewal alongside their fetal-origin counterparts.

1.2.2 Macrophages and the immune system

The two major defenses against pathogens are innate and adaptive immune responses. Innate immunity includes for example cytokines and chemokines that circulate in the bloodstream and leucocytes like macrophages and neutrophils. Innate immunity is faster and more diverse than the adaptive immune response. Components of innate immunity are already present in the blood flow and target tissue so the body's defense reaction to pathogens is rapid. In contrast, a fully active adaptive immune response can be attained after several days. Lymphocytes like T cells are the main factor in adaptive immunity, they are antigen-specific and hold a memory of an antigen encounter. During infection, neutrophils recruit macrophages on site. Pathogen identification requires recognizable pathogen structures, pathogen-associated molecular patterns (PAMPs), and their receptors, pattern-recognition receptors (PRRs). PAMPs can be produced only by microbes and not by eukaryote hosts, be essential for the survival or pathogenicity of the microbe or be invariant structures shared by classes of pathogens (Toews 2009). PAMPs can for example be bacterial carbohydrates or lipoproteins. PRRs are located on the plasma membrane and in the cytoplasmic vesicles of phagocytes (Nash et al. 2015). They include for example mannose receptor and toll-like receptors. Recognition of a PAMP results in the recruitment and activation of macrophages that participate in phagocytosis.

Macrophage migration inhibitory factor (MIF) is an essential part of the innate immune system. Monocytes and macrophages, among other cells, express MIF rapidly after exposure to microbial products and pro-inflammatory mediators and also in response to stress. MIF for example sustains pro-inflammatory function by inhibiting p53-dependent apoptosis of macrophages (Calandra & Roger 2003). Inflammation-associated cytokines lead macrophages to release insulin-like growth factor 1 (IGF-1); Han et al. (2018). The release of that polypeptide hormone occurs during apoptotic cell phagocytosis as well. IGF-1 has its receptor on non-professional phagocytes, like epithelial cells, and binding induces microvesicle uptake but inhibits the annihilation of larger apoptotic cells. The transferring of microvesicles, which macrophages also release, decreases the inflammatory response of epithelial cells.

Macrophages can be categorized by their origin and localization but they can be distributed by their inflammatory features as well. As macrophages have a great plasticity

for environmental signals, activated macrophages are classified into two different groups (Martin & Gurevich, 2021). The stimuli macrophages get from the surrounding tissue are thought to be either pro-inflammatory or anti-inflammatory. Hence, macrophages that have been stimulated by pro-inflammatory conditions are called classically activated macrophages (M1), and when anti-inflammatory conditions have stimulated macrophages, they are called alternatively activated macrophages (M2). It is now more believed that macrophage phenotypes can lie somewhere in-between those two groups and also change their cytokine expression due to chancing conditions (Martin & Gurevich, 2021).

Ferritin, a protein that stores iron, increases iron retention in M1 inflammatory macrophages (Recalcati et al. 2012). The release of iron is blocked because inflammatory stimuli trigger macrophage iron retention by down-regulating the expression of iron exporter ferroportin, which is a transmembrane protein. Ferroportin is probably the only exporter of non-heme iron and it is expressed at high levels for example on macrophages. Retention in macrophages is stimulated by different pro-inflammatory signals. In particular, pro-inflammatory cytokines stimulate macrophage erythrophagocytosis and production of acute-phase protein hepcidin from the liver, which inhibits ferroportin expression and iron excretion (Recalcati et al. 2012). Production of autocrine hepcidin from macrophages can happen as well. Increased iron levels in macrophages lead to defence against invading pathogens.

1.2.3 Macrophages in tissue development and homeostasis

Macrophages have a great capacity to react to microenvironmental signals like endogenous and exogenous molecules around them or to conditional changes in the environment. Based on their studies, Lavin et al. (2014) proposed that macrophage phenotype in tissues is connected to the environment and epigenetic gene expression more than in ontogeny. This high connection means that the anatomical location and function of the tissue create phenotypic adaptations for macrophages under steady-state conditions. For example, microglia contribute to neuronal development and are involved in synaptic remodelling (Gordon & Martinez-Pomares 2017). In addition, macrophages in bone marrow support haematopoiesis and alveolar macrophages contribute to surfactant homeostasis (Gordon & Martinez-Pomares 2017).

On the other hand, it is widely believed that also ontogeny of the macrophages affects their features. In adipose tissue, which has a large number of macrophages, the yolk sac-derived macrophages control adipocyte hypertrophy, but macrophages that are derived from bone-marrow are involved in systematic inflammation (Cox & Geissmann 2020). Macrophages participate in angiogenesis, the formation, growth, and remodelling of new blood vessels from pre-existing vasculature. It is in fact the yolk sac-derived macrophages that promote brain angiogenesis and not monocyte-derived macrophages (Fantin et al. 2010). Fantin et al. (2010) confirmed with their study that embryonic macrophages in the brain were always isolectin B4 (IB4) -positive and that they expressed EGF-like module-containing mucin-like hormone receptor-like 1 (F4/80). F4/80 antigen is a glycoprotein and a core macrophage marker that can be found in cell surfaces from adult mice and it is expressed at a high level on yolk sac-derived macrophages and at an intermediate level in monocyte-derived macrophages. Embryonic macrophages rapidly establish a close association with sprouting vessels in the brain parenchyma. During the formation of subventricular vascular plexus (SVP), macrophages accumulate in the subventricular zone (SZ) and the number of macrophages peak when most of the vascular networking happens. When the SVP is formed, the number of macrophages decreases in the SZ. In contrast, neighboring radial vessels start to form connections between each other when the SZ macrophage population abate. Fantin et al. (2010) also found that when the vascular network is forming, macrophages interact with endothelial tip cells by bridging neighbouring cells.

In mammals, developmentally programmed senescence is followed by macrophage infiltration and the senescent cells are cleared by macrophages (Muñoz-Espín et al. 2013). The senescence process is dependent on p21, which is a kinase inhibitor. Absence of p21 results in senescence loss but is partially compensated by a delayed activation of apoptosis followed by macrophage-mediated clearance. The compensation still results in detectable developmental abnormalities. In the absence of developmentally programmed senescence, Muñoz-Espín et al. (2013) observed a general remodelling mediated by macrophages for example in the endolymphatic sac. Elimination of structures through macrophage-dependent clearance thus plays a great role during development.

Ocular macrophages regulate the shape of the pupils (Takahashi et al. 2020). Macrophages dispose of unnecessary iris debris which results in smooth pupillary edges. If macrophages are absent the pupillary edge ends up being irregular. Pupillary membrane

vessels and hyaloid vessels form the temporary circulatory system in fetal eyes which gradually regress by late gestation in humans (Takahashi et al. 2020). The programmed regression of fetal-type vessels is also controlled by macrophages.

Tissue-resident macrophages occur in great numbers in atrioventricular (AV) nodes and seem to assist normal AV nodal conduction (Hulsmans et al. 2017). Cardiomyocytes, which are responsible for controlling the beating of the heart, drive rhythmic depolarizations in electrotonically coupled macrophages. These macrophages then change the electrophysiological properties of coupled cardiomyocytes. Cell-to-cell interaction is driven by gap junction formation which enables cytoplasm connection. Connexin protein 43 forms the junction between macrophages and cardiomyocyte. The electrotonic load of macrophages depolarizes resting cardiomyocytes, reduces their action potential upstroke velocity and overshoot, and aids early repolarization. These alternations shorten the cardiomyocyte action potential which makes higher rates of conducted beats possible. Sustaining erythropoiesis requires iron and most of it is released by macrophages that recycle iron derived from senescent erythrocytes into the bloodstream through ferroportin (Knutson et al. 2005).

1.2.4 Other macrophage functions

Macrophages are known to be involved in metabolism. For example, it is suggested that macrophages and adipocytes regulate metabolic homeostasis in white adipose tissue by transferring mitochondria from adipocytes to neighboring macrophages *in vivo* (Brestoff et al. 2021). Heparan sulphates control the uptake and it is decreased in obesity. In brown adipose tissue (BAT), macrophages have been shown to secrete neurotrophic factors that promote sympathetic nerve axon branching (Wolf et al. 2017). BAT malfunction in pre-obese mice with mutant macrophages associates with diminished sympathetic innervation and local titers of norepinephrine, which results in lower expression of thermogenic factors by adipocytes. Disruption of the circuit of tissue innervation results in a metabolic imbalance in BAT.

Macrophages play distinct roles in injury and repair. Macrophages induce the destruction of matrix and extracellular structures both directly and indirectly by inducing stromal cells to release matrix metalloproteinases, but macrophages at the same sites possess the ability to aid cell proliferation, secrete and stabilize new matrix components and induce resident cells to secrete matrix components themselves (Duffield 2003). Removal of the

macrophage population in progressive inflammatory injury in the liver causes different results depending on when the deletion is done (Duffield et al. 2005). While ongoing advanced liver fibrosis, the deletion outcomes in reduced scarring and fewer myofibroblasts. In contrast, a failure of resolution with the persistence of cellular and matrix components of the fibrotic response is noticed during recovery when macrophages are removed. Macrophages also participate in wound healing. Healing wounds accumulate iron for effective repair (Wilkinson et al. 2019). Wilkinson et al. found that in healing process, wound macrophages, associated with a prohealing M2 phenotype, stored iron compendiously. *In vitro*, iron is involved in generating differentiation and it also pushes macrophages toward a hypersecretory M2-like polarization state. In dysmetabolic iron overload syndrome (DIOS), macrophage polarization toward the M2 alternative phenotype is impaired but not associated with a pro-inflammatory profile (Lahaye et al. 2021). The up-regulation of transferrin receptor 1 in DIOS macrophages suggests an adaptive role that may limit iron toxicity in DIOS. It is also suggested that macrophages directly contribute collagen to the forming scar (Simões et al. 2020).

1.2.5 Examples of tissue-resident macrophages

Four different subsets of macrophages can be found in the spleen. The spleen, which is identified as a blood-filtering organ, has two main types of tissues: white pulp and red pulp. White pulp is a lymphatic tissue containing mostly white blood cells like T and B cells and red pulp consist of blood-filled cavities and splenic cords. The white pulp locates highly phagocytic macrophages which are part of the immune response, while metabolic red pulp macrophages are involved in homeostatic and metabolic functions erythrocyte phagocytosis and iron recycling (A-Gonzalez & Castrillo 2018). Between the red and the white pulp is the marginal zone which is mainly composed of intermediate-sized lymphocytes (Kraal G. 1992). Two populations of immune response-related macrophages are located in the marginal zone: marginal metallophilic macrophages (MMM) and marginal zone macrophages (MZM) (A-Gonzalez & Castrillo 2018). Both macrophage populations are responsible for the clearance of blood-borne encapsulated bacteria and parasite phagocytosis. Few microanatomical environments have coexisting macrophage populations that are phenotypically and functionally different from each other. Backer et al. (2010) studied that MMMs are potential antigen-presenting cells as MMMs can specifically take up antigens, transfer them to $CD8^+$ T cells and lastly activate dendritic cells. MMMs also interact with nearby cells: Nolte et al. (2004) studied that the release of LTαβ from follicular B cells keeps up the maintenance of MMMs. In addition, Liu et

al. (2014) showed that follicular B cells travel towards the marginal zone when getting stimulation from oxysterols and suggested that MMMs produce those oxysterols. MZMs phagocytose effectively blood-borne apoptotic cells but they also express SIGN-R1 molecule that has been shown to be crucial between marginal zone B-cells and MZM interaction (A-Gonzalez & Castrillo 2018). The B cells inflict germinal center reaction by traveling to the follicles in the white pulp after they have recognized antigens. B cells present antigens to follicular dendritic cells, but if there is no SIGN-R1 present, the cells cannot migrate to the follicles. The different macrophage subsets of the spleen can reprogram some of their functions, but more importantly, the environmental signals determine how they function.

Among all organs, the liver has the largest number of macrophages. The role of macrophages as homeostasis maintainers is crucial in the liver. The liver is comprised of self-maintaining, non-migratory tissue-resident phagocytes, Kupffer cells, and monocyte-derived macrophages (Krenkel & Tacke 2017). Kupffer cells originate from yolk sac-derived precursors during embryogenesis. The cells sustain homeostasis through metabolic activities, getting rid of microbial particles and redundant cellular components. Kupffer cells also induce immunological tolerance by modulating inflammation and recruiting immune cells to the liver. In response to local signals originating from example from a liver injury, both Kupffer cells and monocyte-derived macrophages adapt their phenotypic behaviour to minimize the damage. Even though both macrophage subsets in the liver share many features in common, some functional differences exist despite their different origin. The phagocytic activity of macrophages in the liver is regulated by the vagus nerve (Fonseca et al. 2019). Beattie et al. (2016) showed that in genotoxic injury, yolk sac-derived Kupffer cells accumulated acetylated low-density lipoproteins better but were poorer to uptake a range of bacterial pathogens.

1.3 Macrophages in the pituitary

Macrophages can be identified in the pituitary gland, for example, by their specific antibody for ionized calcium-binding adaptor molecule 1 (Iba1), which is a macrophage-specific calcium-binding protein (Zhao et al. 2020, Yagasaki et al. 2021). Zhao et al. (2020) identified macrophages in the anterior lobe, while Yagasaki et al. (2021) studied the whole pituitary and found macrophages from the anterior and posterior lobe while the intermediate lobe had few macrophages. Chronic inflammatory pain increases the number

of macrophages, but it is still unclear where they are coming from (Yagasaki et al. 2021). Resident macrophages in the anterior pituitary can proliferate or macrophages can migrate through blood vessels due to increased permeability. The same study showed that the level of interleukin-1 beta (IL-1β) in the anterior lobe increased during chronic inflammation pain and most of the IL-1β-positive cells (nearly 90 %) were macrophages. IL-1β is an important cytokine in monocyte activation and it is also involved in pro-inflammatory activation in peripheral tissues and the brain.

The two macrophage classes, classically activated (M1) and alternatively activated (M2), has been shown to be both present in the rat anterior pituitary gland (Fujiwara et al. 2017). M1 macrophages are involved in infection response and enhance inflammation while M2 macrophages promote angiogenesis and tissue remodelling induced by cytokines interleukin 4 or 13. M2 macrophages also down-regulate functions derived from M1 activity. Marques et al. (2019) showed that pituitary neuroendocrine tumors have increased macrophage content. Those tumors are an active source of cytokines, which stimulate macrophages, neutrophils and lymphocyte migration into the microenvironment of the tumor. From the two macrophage classes, M2 dominates the macrophage numbers in the tumor while M1 is more common in the normal pituitary (Marques et al. 2019). The ratio of macrophages (M2:M1) positively correlated with the micro vessel density and the area in pituitary neuroendocrine tumors, which is rational due to the angiogenesis promotion the M2 class is suggested to have.

Studies of macrophages in the pituitary and how they are regulated in the tissue can be found. However, little is known about the connection between macrophages and hormone-releasing cells. Especially the impact macrophages have on the hormone-releasing cells is still unclear.

1.4 Aims of the study

The aims of the study are to define, with the help of knock-out mice strains, the impact of macrophages on the hormone-releasing cells in mouse pituitary and to clarify if macrophages and the hormone-releasing cells share the same intratissue localization. Using knock-out mouse strains along with wild-type mice gives the opportunity to compare differences, and thus, to get insight not only in the consequences the gene

deletion of a specific macrophage or monocyte population cause, but also in the normal state in the tissue.

Suitable knock-out strains for this study were Plvap, CCR2 and Nur77. In Plvap knock-outs, the *Plvap* gene, that codes protein called plasmalemmal vesicle associated protein-1, is inoperative. Plvap$^{-/-}$ mice do not have fetal liver macrophages and previous unpublished data from Rantakari research group of decreased hormone levels suggests that in this study the results would show a decreased number of hormone-producing cells in the pituitary. The nuclear orphan receptor (Nur77) is deficient in the Nur77 knock-outs and CCR2 knock-out mice lack C-C chemokine receptor type 2 (CCR2) protein. Murine CCR2 has a remarkable role in macrophage recruitment, and thus, there might be differences in the macrophage populations in the knock-out pituitary compared to a wild-type one, which could affect the hormone-releasing cells as well. Differences might also be seen in the Nur77$^{-/-}$ mice since they lack Ly6C^{low} monocytes. These monocytes are patrolling monocytes that express low levels of lymphocyte antigen 6C and take part in inflammation responses and tissue repair. In contrast, Ly6C^{high} monocytes are CCR2 positive. Since some of the macrophages derive from monocytes, the lack of monocyte-derived macrophage populations might cause an impact on the development and functions of the pituitary in these knock-out models.

2 MATERIALS AND METHODS

In order to study macrophages and hormone-releasing cells and their intratissue localization, three different methods were used. First, RNAscope®, which is an *in situ* hybridization assay for detecting target RNA within intact cells, was used to evaluate macrophage-specific gene expression and localization in the pituitary of wild-type mice. Second, alongside macrophages, hormone-releasing cells were studied with immunofluorescence staining, comparing the number of active hormone-releasing cells between wild-type mice and a knock-out strain. Third, histological differences in the anterior pituitary gland between wild-type mice and two knock-out models were compared. These changes were visualized by staining the tissues with haematoxylin and eosin solutions.

2.1 Animals

Mice were housed under controlled environmental conditions (12 hours light/12 hours darkness, at 21 ± 3 °C and humidity 55 ± 15 %) at the Central Animal Laboratory of the University of Turku. All animal experiments were approved by the National Animal Experiment Board in Finland.

Four different mouse strains were used and altogether five different age groups (Table 1). C57BL/6NRj mice were in every experiment. C57BL/6 is the most well-known inbred mouse strain and C57BL/6NRj is one of its substrains. Also, a knock-out mouse strain, Plvap$^{-/-}$, was used in the immunofluorescence staining experiment, and two knock-out mouse strains, CCR2$^{-/-}$ and Nur77$^{-/-}$, were used in the morphology studies. All five time-points were included in the RNAscope® assay while immunofluorescence staining was done for 5-week-old samples and haematoxylin and eosin staining for 8-week-old samples only. All experiment mice were males.

Table 1. Different mouse strains and time-points used in the experiments.

Experiment	Mouse strains	Time-points
RNAscope® assay	C57BL/6NRj	Newborn, 1, 3, 5, and 8 wk
Immunofluorescence staining	C57BL/6NRj, Plvap	5 wk
Haematoxylin & eosin staining	C57BL/6NRj, CCR2, Nur77	8 wk

2.2 Sample collection and preparation

Paraffinized pituitaries mounted on slides were used throughout the experiments. Pituitaries from 5-week-old C57BL/6NRj mice used in the RNAscope® assay and in the immunofluorescence staining were collected earlier and processed for paraffin blocks. Other samples were collected and processed as follows. Mice were euthanised by carbon dioxide asphyxiation and cervical dislocation. Pituitaries from newborn and 1-week-old mice were collected still attached to the bottom of the skull and put in 10 % normally buffered formalin for approximately 30 minutes and then cut from the skull base submerged in phosphate buffered-saline (PBS). After the detachment, the pituitaries were put back in formalin which was changed in case it contained a notable amount of blood or tissue residues from other parts of the skull base. Pituitaries were fixed at room temperature (RT) overnight (o/n). Pituitaries dissected from mice that were 3 to 8 weeks old, were cut directly from the skull base and immediately fixed in formalin (RT, o/n) or in 4 % paraformaldehyde, PFA (+4 °C, o/n). Two pituitaries from $CCR2^{-/-}$ mice and one from a $Nur77^{-/-}$ mouse were fixed with PFA and used for haematoxylin and eosin staining. After fixation, the pituitaries were treated with 50 % ethanol for 30 minutes and then the ethanol was changed to 70 % ethanol. The pituitaries were collected to tissue cassettes between polyester plastic foam biopsy pads and submerged in fresh 70 % ethanol. The cassettes were then placed at +4 °C until the paraffin embedding process. The paraffin embedding was done in the Histology core facility in Medisiina D, University of Turku.

Paraffin blocks were stored at RT and the embedded pituitaries were cut with microtome (Leica RM2255) to 5 µm thick sections. Sections were placed in lukewarm water and then onto SuperFrost Plus® slides with one to several pituitary sections on one slide. Tissue slides were also carefully dipped into +47 °C water bath to straighten the tissue sections and to get the paraffin attach to the slide surface. All the slides were finally put at +37 °C to dry completely. After one to three nights the slides were placed at RT.

2.3 RNAscope® Multiplex Fluorescent Reagent Kit v2 Assay

The RNAscope® assays are staining methods which can be used to visualize RNA molecules in tissue samples that are mounted on slides. RNA-specific probes hybridize to target RNA which are then treated with signal amplification molecules. The signals are created by using different fluorescent Opal™ dyes. For result observation, either standard bright field microscope or fluorescent microscope can be used. There are single-plex, 2-

plex, multiplex and automated RNAscope® assays available. With a 4-plex assay, up to four different RNA targets can be visualised at once. RNAscope® assay can be done for formalin-fixed paraffin-embedded, fresh frozen or fixed frozen tissues, tissue microarray and cultured cells.

Single-cell RNA sequencing data from Rantakari research group (unpublished) was to be validated with RNAscope® method. The method was to study different macrophage populations in the pituitary, their localization and especially macrophage markers, which have no functional antibodies to use for fluorescence-activated cell sorting (FACS) or in immunofluorescence staining. In this study, a 4-plex RNAscope® assay and formalin-fixed paraffin-embedded tissues from C57BL/6NRj mice were used. The four chosen target genes were platelet factor 4 (*Pf4*), high affinity immunoglobulin gamma Fc receptor I (*Fcgr1*), mannose receptor C-type 1 (*Mrc1*) and secreted protein acidic and rich in cysteine (*Sparc*). The RNA sequencing data suggests that *Pf4* is a macrophage marker for embryonic macrophages. In the data, *Mrc1* and *Sparc* both define one macrophage population and for *Sparc* not any working antibody was found as the signal was not specific. *Fcgr1*, which encodes the CD64 Fc γ receptor, is specific for macrophages so it can be considered as a core macrophage marker. Therefore, it was included in the experiment to specify if other probe signals would actually be from macrophages and not from other cells. Also, DAPI (4′,6-diamidino-2-phenylindole) was used to stain nuclei as the stain binds strongly to adenine-thymine-rich regions in the DNA. RNAscope® Multiplex Fluorescent Reagent Kit v2 was used alongside the specific probe mix kit. The Opal™ dyes were Opal™ 520, Opal™ 570, Opal™ 620 and Opal™ 690 as instructed.

2.3.1 Assay preparation

All the preparations were done following the RNAscope® user manual provided by ACDBio. First 20X saline sodium citrate (SSC) and 1X wash buffer were prepared. SSC was prepared by dissolving 175,3 g of NaCl and 88,2 g of sodium citrate in 800 ml of milli-Q water. PH was adjusted to 7 with a few drops of 1 M HCl and the total volume to 1 l with additional milli-Q water. SSC was then sterilized by autoclaving and stored at room temperature. Wash buffer was prepared by first warming one bottle (60 ml) of RNAscope® 50X wash buffer up to 40 °C in a water bath for approximately 20 minutes and then dissolving it to 2,94 l of milli-Q water.

75 µl of DMSO was added into all four Opal™ dye tubes (520, 570, 620 and 690) and the tubes were placed at + 4 °C. The positive and negative control probe solutions were included in the kit and were ready-to-use mixtures for a 3-plex assay. The positive control probe was a mixture of three probes targeting *POLR2A* in channel 1 (C1), *PPIB* in C2 and *UBC* in C3. The negative control probe was targeting a mixture of bacterial gene *DapB*, while each detection channel had its own negative control probe. Since using the 4-plex assay, 60 µl of Mm-HPRT-C4 was added to the positive control bottle (3 ml) after being warmed up to 40 °C for 10 minutes. Also 60 µl of DapB-C4 was added to the negative control probe bottle (3 ml) after the same warming up process. These prepared control probes were stored at +4 °C.

2.3.2 Validation and optimization of the RNAscope® assay

RNAscope® method was first tested with Control Slides and Control Probes provided for the proper validation of the kit. The technical control included mouse 3T3 cell pellet slides, which were treated either with a non-specific bacterial negative control probe mix and with a low-copy housekeeping gene-positive control probe mix. When the assay works properly, technical controls will show clean negative control probe staining and strong positive control probe staining.

The assay was executed using the modified instruction manual by ACDBio (Appendix 1). HYBEZ™ Oven, which included HybEZ™ Humidity Control Tray, was used throughout the assay first at 60 °C when baking the slides, then at 40 °C with other incubations. For 40 °C incubations a humidifying paper wet with milli-Q water was placed inside the tray. The manual instruction included using distilled water in specific steps but milli-Q water was used instead. A total of 700 ml of RNAscope® 1X Target Retrieval Reagent was prepared for boiling the slides and ImmEdge™ hydrophobic barrier pen was used to draw a barrier around the dried tissue sections. Barriers were left to dry for approximately 30 minutes. During AMP hybridization Opal™ dyes were diluted with TSA buffer using an instructed starting dilution of 1:1500. The volume needed for each section was determined to be 150 µl so 0,5 µl of each dye was diluted to 750 µl of TSA and then placed in the dark. HRP-C signal development was done so that C1 (*Pf4*) was combined with Opal™ 520, C2 (*Fcgr1*) with Opal™ 570, C3 (*Mrc1*) with Opal™ 620 and C4 (*Sparc*) with Opal™ 690. DAPI incubation time was set to 30 seconds and ProLong® Gold Antifade Mountant was used for mounting. Slides dried overnight in

the dark and were then stored at +4 °C. Imaging was done with ZEISS LSM780 confocal microscope and Midi Fluorescence slide scanner.

After validation of the RNAscope® method, the assay optimization was carried out with 5-week-old pituitary samples. Since different HRP-channels were tested with different Opal™ dyes, two sets of assays were needed (Table 2). *Fcgr1* target was first combined with Opal™ 570 and then in the 2nd staining with Opal™ 620. Accordingly, *Mrc1* was first stained with Opal™ 620 and then with Opal™ 570. Other targets were combined with the same dyes in both staining sets. Both sets had one positive control slide, one negative control slide and two target slides. Target slides needed target probe mix which was prepared before the assay. *Pf4*-C1 bottle (3 ml) and *Fcgr1*-C2, *Mrc1*-C3 and *Sparc*-C4 tubes (60 µl each) were warmed up to 40 °C in a water bath for 10 minutes. C2, C3 and C4 were then added to C1 bottle with a pipette to get one mixture. The probe mix was stored at +4 °C. Both assays were done as the control slide test assay and imaged again with the confocal microscope and the slide scanner. Control slides were treated with proper control mixes and target slides with the target probe mix.

Table 2. Different HRP-Opal™ combinations and used detection channels for the test slide (5-week-old pituitary samples) assays.

Detection channel	**Opal™ fluorophore**	**1st staining experiment (target + dye)**	**2nd staining experiment (target + dye)**
DAPI	-	-	-
FITC	520	HRP-C1 (*Pf4*) + 520	HRP-C1(*Pf4*) + 520
TRITC	570	HRP-C2 (*Fcgr1*) + 570	HRP-C3 (*Mrc1*) + 570
Texas Red	620	HRP-C3 (*Mrc1*) + 620	HRP-C2 (*Fcgr1*) + 620
Cy5	690	HRP-C4 (*Sparc*) + 690	HRP-C4 (*Sparc*) + 690

The slide scanner did not have a suitable channel option for Opal™ 620, and with a confocal microscope, Texas Red and TRITC channels turned out to be overlapping remarkably, so Opal™ 620 was not used anymore in the following assays. Because of the small size of the pituitary sections, some of the reagent amounts in the protocol were decreased by a few drops and Opal™ amounts were adjusted to 100 µl/ slide.

To minimize autofluorescence, an autofluorescence quenching procedure was added to the RNAscope® assay. Vector® TrueVIEW™ Autofluorescence Quenching Kit (Vector

Laboratories) was tested with four pituitary slides: positive and negative control slides were from 5-week-old pituitaries and two target probe slides were from 1-week-old pituitaries. The assay was done as previously but Opal™ 620 was not used. The staining set combinations used in this test were HRP-C1 with Opal™ 520, HRP-C2 with Opal™ 570 and HRP-C4 with Opal™ 690. User guide from Vector Laboratories was used for the quenching kit testing (Appendix 2). Reagent preparation was done during the assay so that the final mix had a 1:1:1 volume ratio of the three different reagents. The volume for pituitary sections was decided to be kept same as with the Opal™ dyes (100 µl) so 40 µl of each reagent was used in total. Incubation time for the mixture was set to 3.5 minutes and incubation time for DAPI was increased to 60 seconds. The quenching kit included VECTASHIELD® Vibrance™ Antifade Mounting Medium and it was tested alongside ProLong™ Gold which was used in the earlier assay tests. The positive control slide and one target slide were mounted with VECTASHIELD® and the negative control slide and the other target slide with ProLong™ Gold. The quenching kit was included in the following RNAscope® assay experiments as well. From the two mounting media, ProLong™ Gold was replaced by VECTASHIELD®.

2.3.3 RNAscope® detection of RNA targets from pituitary samples

After testing and optimization, RNAscope® assay was done with pituitary samples from C57BL/6NRj newborn and 1 week to 8 weeks old mice (Table 1). There were three staining set experiments in total (Table 3). All the sets had 5-week-old pituitary control slides and two target slides from each time-point. The assay was done as previously, but this time the autofluorescence quenching kit procedure was included in the protocol and the target retrieval amount was halved. Imaging was done with LSM780 and LSM880 confocal microscope (ZEISS). LSM780 was used to take close-up images from the first two sets with C-Apochromat 40X/ 1,20 W Korr M27 objective. LSM880 was used to get close-up images from the third staining set with Plan-Apochromat 40X/ 1,2 Imm Corr DIC M27 objective and overview images from all the sets with Plan-Apochromat 20X/ 0,8 M27 objective using tile scan property. Images were further processed with Fiji software (Schindelin et al. 2012) by changing the channel colours and adjusting brightness and contrast of the signals.

Table 3. Different HRP-Opal™ combinations and used detection channels for all time-point RNAscope® assays.

Detection channels	Opal™ fluorophore	1st staining experiment (target + dye)	2nd staining experiment (target + dye)	3rd staining experiment (target + dye)
DAPI	-	-	-	-
FITC	520	HRP-C1 (*Pf4*) + 520	HRP-C1 (*Pf4*) + 520	HRP-C2 (*Fcgr1*) + 520
TRITC	570	HRP-C2 (*Fcgr1*) + 570	HRP-C2 (*Fcgr1*) + 570	HRP-C3 (*Mrc1*) + 570
Cy5	690	HRP-C4 (*Sparc*) + 690	HRP-C3 (*Mrc1*) + 690	HRP-C4 (*Sparc*) + 690

2.4 Immunofluorescence staining

The number of hormone-releasing cells in the pituitary of Plvap knock-out mice and wild-type mice at the age of 5 weeks was compared using immunofluorescence staining in paraffin sections. In Plvap$^{-/-}$ the fetal liver macrophages are missing. Comparing wild-type and knock-out mice would clarify if the macrophage deficiency affect the hormone production of the hormone-releasing cells. Target hormones were growth hormone (GH), luteinizing hormone (LH), prolactin (PRL) and thyroid-stimulating hormone (TSH). Antibodies targeting the hormones and their final dilutions can be seen in Table 4. Nuclei were also stained using DAPI stain.

Table 4. Antibodies used in the immunofluorescence staining experiment and their dilutions/concentrations.

Primary antibody/Host/Manufacturer, #	Final dilution
Anti-rat-GH/Rabbit/NIDDK, #AFP-5672099	1:1000
Anti-rat-LH beta/Rabbit/NIDDK, #AFP-C697071P	1:1000
Anti-mouse-PRL/Rabbit/NIDDK, #AFP-879151	1:2000
Anti-rat-TSH/Rabbit/NIDDK, #AFP-127489	1:1000
Secondary antibody/Host/Manufacturer, #	**Final concentration**
Anti-rabbit/Goat/Invitrogen, #A27040	2 µg/ml

Staining protocol was done four times in total. In addition to the hormones, EFG-like module-containing mucin-like hormone receptor-like 1 (F4/80) was decided to be targeted. Since F4/80 antigen is expressed on macrophages, including microglia, signal from F4/80 helps to detect the connection between positive hormone-releasing cells and macrophages. The antibodies targeting F4/80 and their concentrations can be seen in Table 5. Each sample slide had three tissue sections from which two were used as target sections for one hormone and F4/80, and one was used as a secondary control. First staining experiment was done using two wild-type pituitary samples, both fixed in 4 % PFA. GH and PRL were the targeted hormones. A conjugated antibody was used for F4/80 detection. Set concentration for the conjugate was 2 µg/ml.

Table 5. Antibodies for the immunofluorescence staining and their dilutions/ concentrations for the experiment. 4th staining experiment targeted only the four hormones and F4/80 was left out.

Staining experiment	**Antibodies targeting F4/80**	**Antibody concentration**
1. staining	F4/80-A488 clone, BM8 ref. 53-4801-82	2 µg/ml
2. staining	F4/80-A488 clone, BM8 ref. 53-4801-82	10 µg/ml & 20 µg/ml
3. staining	Primary: anti-mouse F4/80/ Bio X Cell, #BE0206 Secondary: Anti-rat A546/ Goat/ Life Technologies, #A11081	20 µg/ml 10 µg/ml
4. staining	-	-

The second staining was done again with two wild-type pituitary samples with higher F4/80-A488 antibody concentrations. Target hormone was only GH, with the same antibody dilutions, F4/80 were tested with both 10 µg/ml and 20 µg/ml concentrations. Detailed protocol for the first and second staining experiments is in Appendix 3.

During the third staining experiment primary and secondary antibodies for detecting F4/80 were used. Final concentration for the primary antibody was 20 µg/ml and for the secondary antibody 10 µg/ml. Wild-type samples were used and GH was the target hormone. Changes to the protocol were added based on earlier immunofluorescence staining protocols by the group. The modified protocol is in Appendix 4. In the final staining, only the four hormones were targeted leaving F4/80 out due to detection

problems. The staining included three Plvap knock-out samples and three wild-type samples. Hormones were targeted using separate slides per hormone, so four slides in total were used from each mouse individual. The experiment followed the latter, modified protocol, but the secondary antibody incubation was at room temperature. All the sample slides were imaged with ZEISS LSM880 confocal microscope and the last slide set from the 4th staining was also scanned with a Pannoramic Midi fluorescence slide scanner. Positive hormone-releasing cells were counted and the numbers were compared between the knock-out and wild-type mice. Counting was done from the slide scanner images using CaseViewer 2.4. A t-Test (Two-Sample Assuming Unequal Variance) was done to the cell-counting results.

2.5 Haematoxylin & eosin staining

Histological tissue differences of 8-week-old mice between C57BL/6NRj, $CCR2^{-/-}$ and $Nur77^{-/-}$ mice were studied. Since CCR2 is involved in macrophage recruitment and Nur77 knock-outs are missing the $Ly6C^{low}$ monocytes, the macrophage populations in pituitary might be affected and the morphological appearance change. Three animals were used from each strain. Pituitaries were fixed in either 4 % PFA or 10 % normally buffered formalin. The fixation difference was only due to availability. Leica RM2255 microtome was used to cut 5 µm thick sections from the tissues. Each sample slide was covered with several pituitary tissue sections and 1 to 2 sample slides were stained from each animal using a standard staining protocol by Rantakari research group (Appendix 5). The protocol was first tested with two C57BL/6NRj pituitary sample slides so that the eosin incubation time was 45 seconds instead of 30 seconds. Other slides were stained with an incubation of 30 seconds. All stained samples were imaged with Pannoramic 250 Flash slide scanner.

3 RESULTS

With optimization and a few adjustments, results were obtained from every method. Still, some of the RNAscope® probes did not work properly and the signal strengths varied. The three sets ensured signals from the target probes since every probe was involved in the different sets at least twice. Immunofluorescence staining worked well for the hormone-releasing cells and the signals were strong and clear so the cell calculation could be done without a problem. Unfortunately, macrophages could not be detected alongside the hormonal cells since signal from the designated macrophage marker could not be attained. Haematoxylin and eosin stains gave clear results and from the images it was possible to identify different cell types and other cell structures in the anterior part of the pituitary sections.

3.1 RNAscope® method results

RNAscope® staining method was used for three staining sets and four target probes in total (Table 3). The four targets were mixed between the sets to get different target combinations since only three different Opal™ fluorophores could be detected at once. Nuclei were also stained alongside target probes with DAPI and the staining was successful in every set. The images were processed to collages by age groups which were newborn, 1 week, 3 weeks and 8 weeks. Control images (pituitary sections from 5-week-old mice) can be found in Appendix 6.

3.1.1 1st staining experiment

In the first staining set the target probes were *Pf4*, *Fcgr1* and *Sparc*. *Pf4* and *Fcgr1* were not visible in any age group (Figures 4 and 5). The control images refer to the fact that the staining was not successful with the two probes (Appendix 6A). *Sparc* also gave a blank signal in the positive control (5 weeks) but in the target images there were clear signal. The signal from newborn to 3 weeks was mostly from structural staining. Nonetheless, since the core macrophage marker, *Fcgr1*, did not work, the signal from *Sparc* could not be identified to actually be from macrophages.

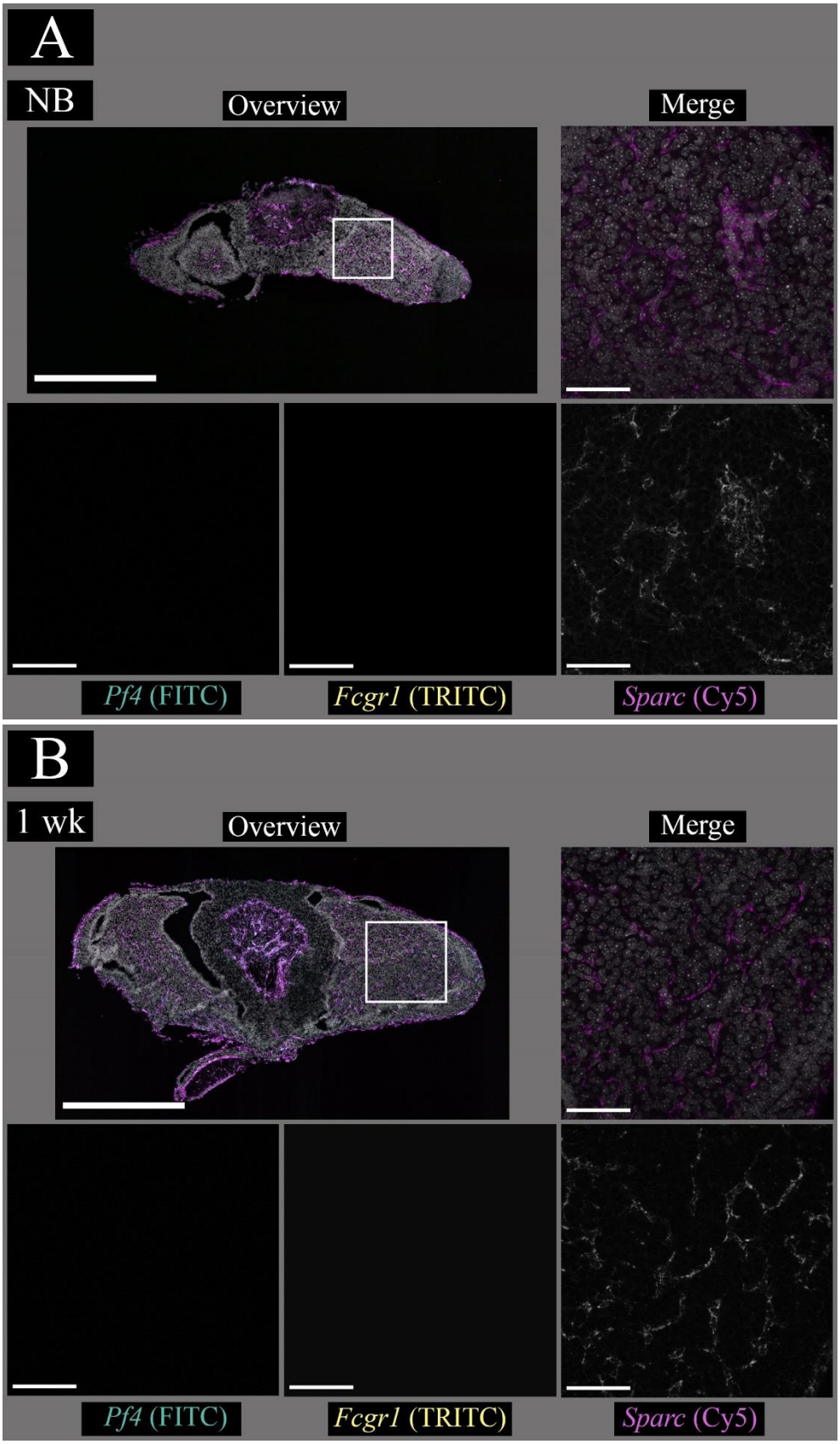

Figure 4. Pituitary sections from (A) a newborn C57BL/6NRj mouse and (B) a 1-week-old C57BL/6NRj mouse from the 1st staining experiment. The scale bar in the overview images is 400 µm and in the close-ups, from the regions of interest, 50 µm. The colour of the targets in the overview and merge images are specified by the colours of the target name. The signal from nuclei is in grayscale in the overview and merge images.

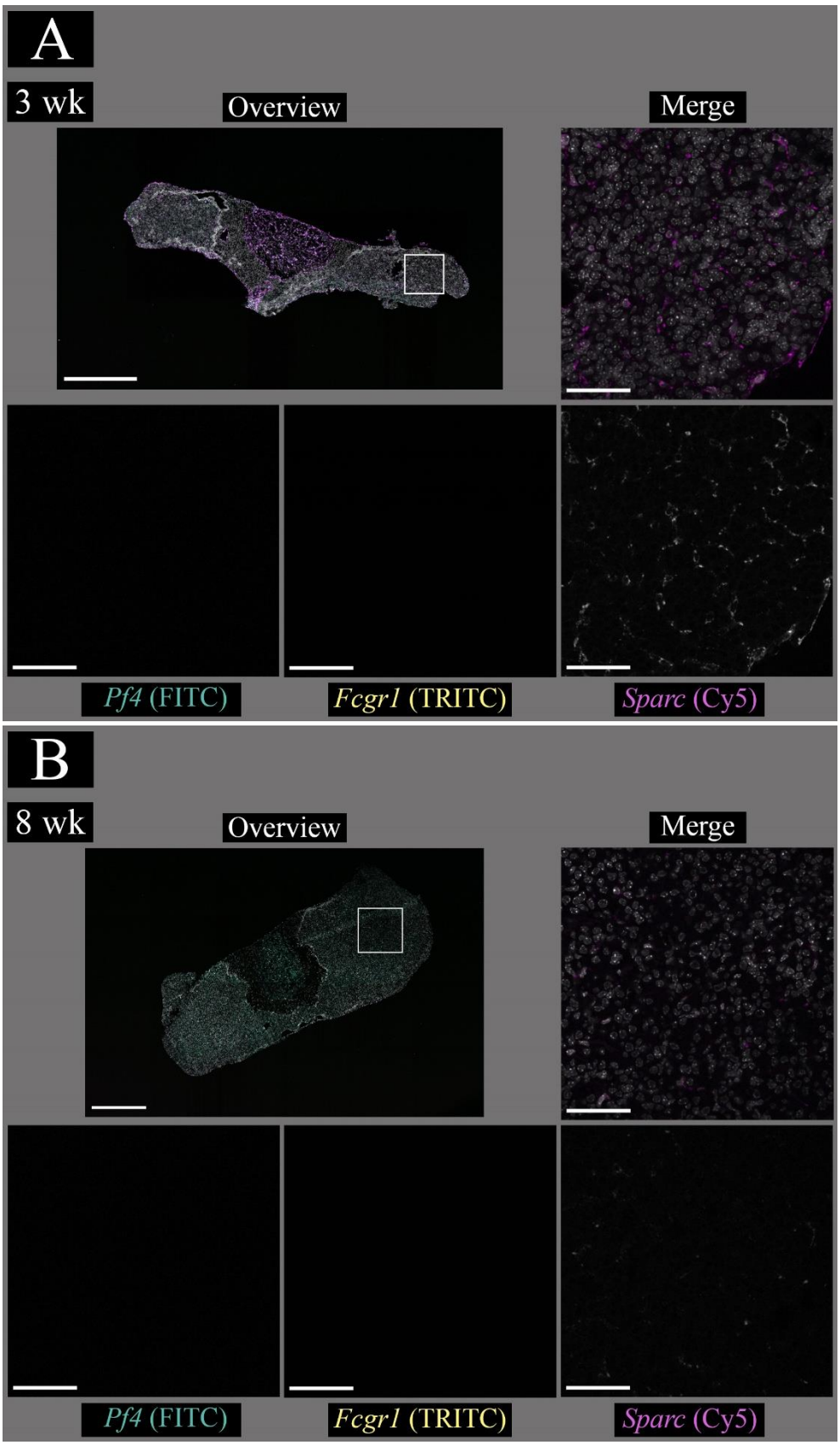

Figure 5. Pituitary sections from (A) a 3-week-old C57BL/6NRj mouse and (B) an 8-week-old C57BL/6NRj mouse from the 1st staining experiment. The scale bar in the overview images is 400 µm and in the close-ups, from the regions of interest, 50 µm. The colour of the targets in the overview and merge images are specified by the colours of the target name. The signal from nuclei is in grayscale in the overview and merge images.

3.1.2 2nd staining experiment

Probes for the second staining set were again *Pf4* and *Fcgr1*, but with these two, *Mrc1* was the third target. This time, some faint *Fcgr1* signals could be seen in all time-points but they appeared to be nonspecific. A proper *Pf4* signal could be detected which was stronger in the newborn and 1-week pituitaries. As *Fcgr1* did not work, it was again impossible to say which signal came spesifically from macrophages. There was no visible signal from *Mrc1* in any age group (Figures 6 and 7). The positive control image seemed to have only background signal which means that the staining did not work properly for the target (Appendix 6B).

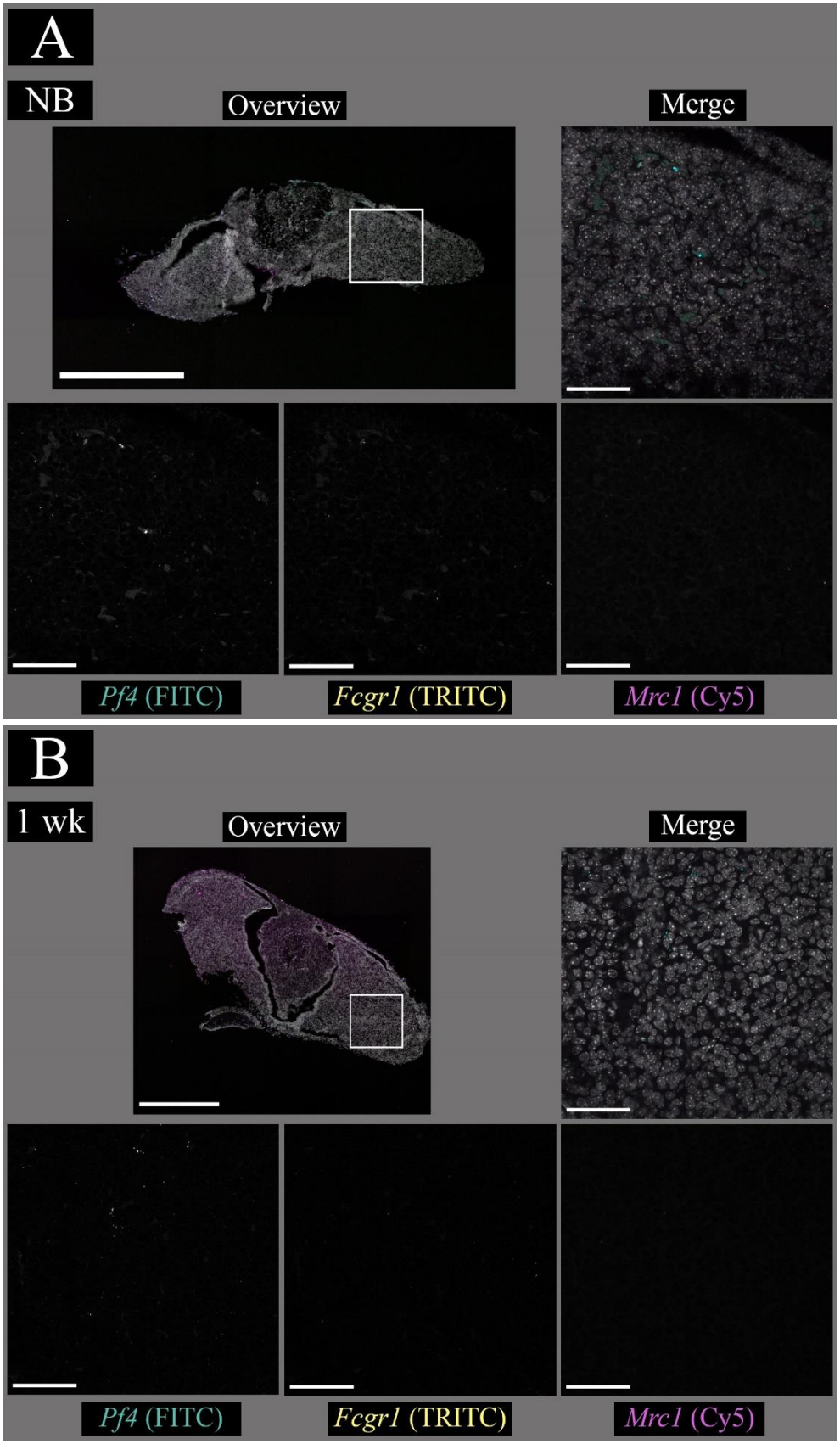

Figure 6. Pituitary sections from (A) a newborn C57BL/6NRj mouse and (B) a 1-week-old C57BL/6NRj mouse from the 2nd staining experiment. The scale bar in the overview images is 400 µm and in the close-ups, from the regions of interest, 50 µm. The colour of the targets in the overview and merge images are specified by the colours of the target name. The signal from nuclei is in grayscale in the overview and merge images.

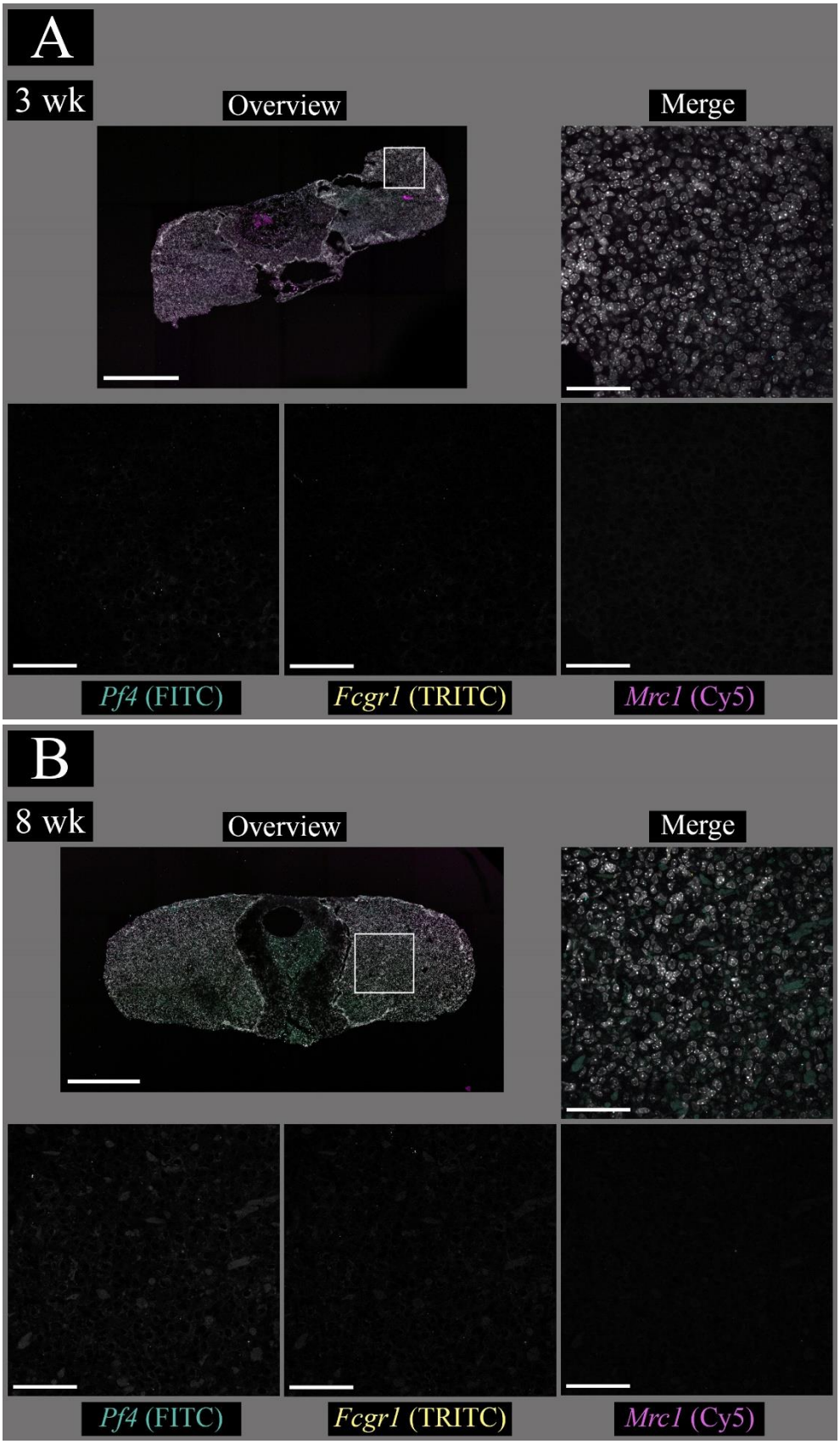

Figure 7. Pituitary sections from (A) a 3-week-old C57BL/6NRj mouse and (B) an 8-week-old C57BL/6NRj mouse from the 2nd staining experiment. The scale bar in the overview images is 400 µm and in the close-ups, from the regions of interest, 50 µm. The colour of the targets in the overview and merge images are specified by the colours of the target name. The signal from nuclei is in grayscale in the overview and merge images.

3.1.3 3rd staining experiment

For the last staining experiment the target combination was *Fcgr1*, *Mrc1* and *Sparc*. All the probes gave signal this time (Figures 8 and 9). All the positive control images for the third experiment showed a fair amount of signal from every probe as well so the staining appeared to be successful at first (Appendix 6C). As the positive signal from the probes seemed to come from the same place in the tissue section it would seem that all the macrophages express the *Sparc* gene. However, the RNA sequencing data has shown that only few macrophages in the pituitary are positive for *Sparc*. This suggests that the *Fcgr1* macrophage marker did not work properly and thus we cannot say if the signal from *Mrc1* is noteworthy either.

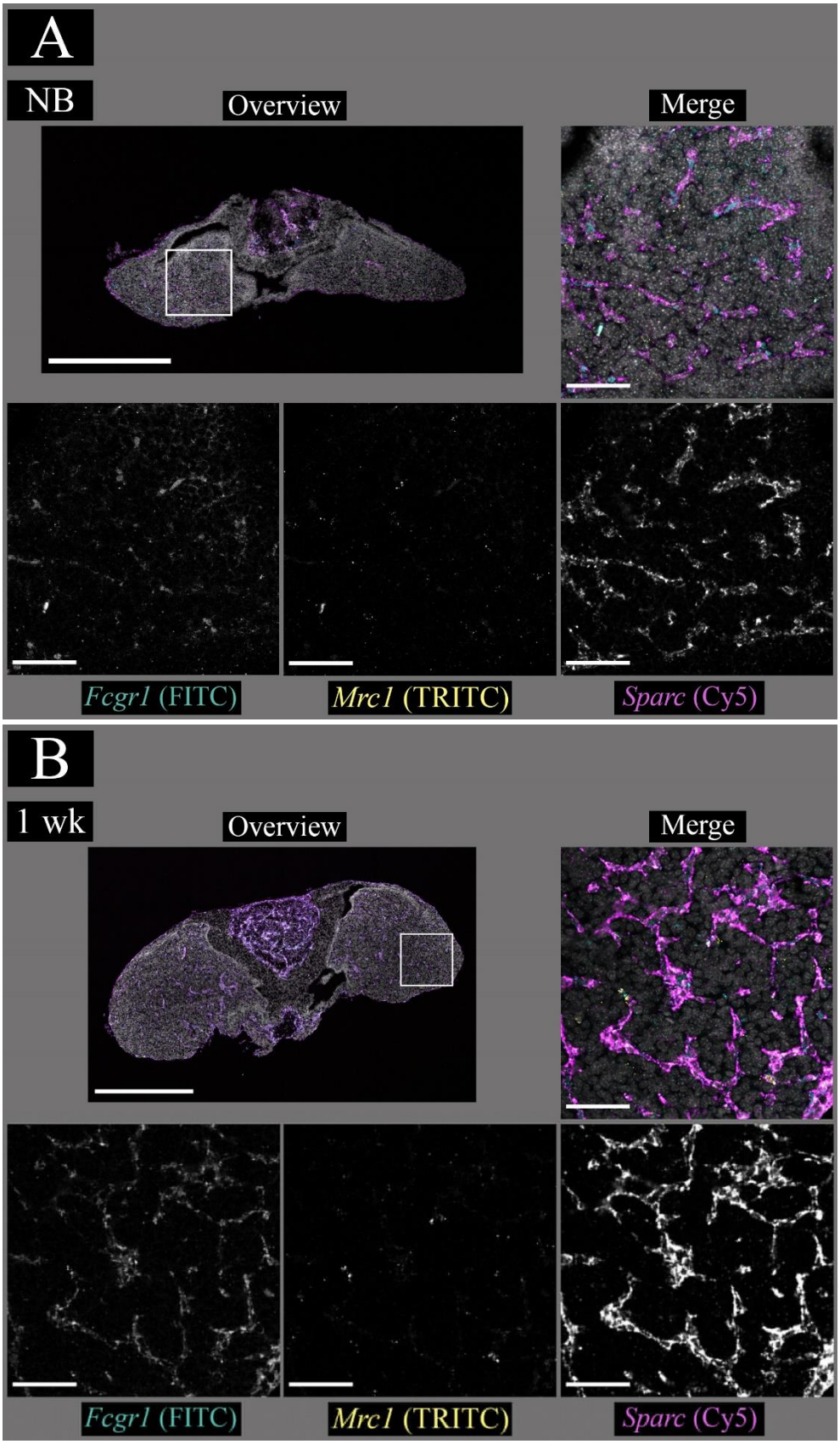

Figure 8. Pituitary sections from (A) a newborn C57BL/6NRj mouse and (B) a 1-week-old C57BL/6NRj mouse from the 3rd staining experiment. The scale bar in overview images is 400 µm and in close-ups, from the regions of interest, 50 µm. The colour of the targets in the overview and merge images are specified by the colours of the target name. The signal from nuclei is in grayscale in the overview and merge images.

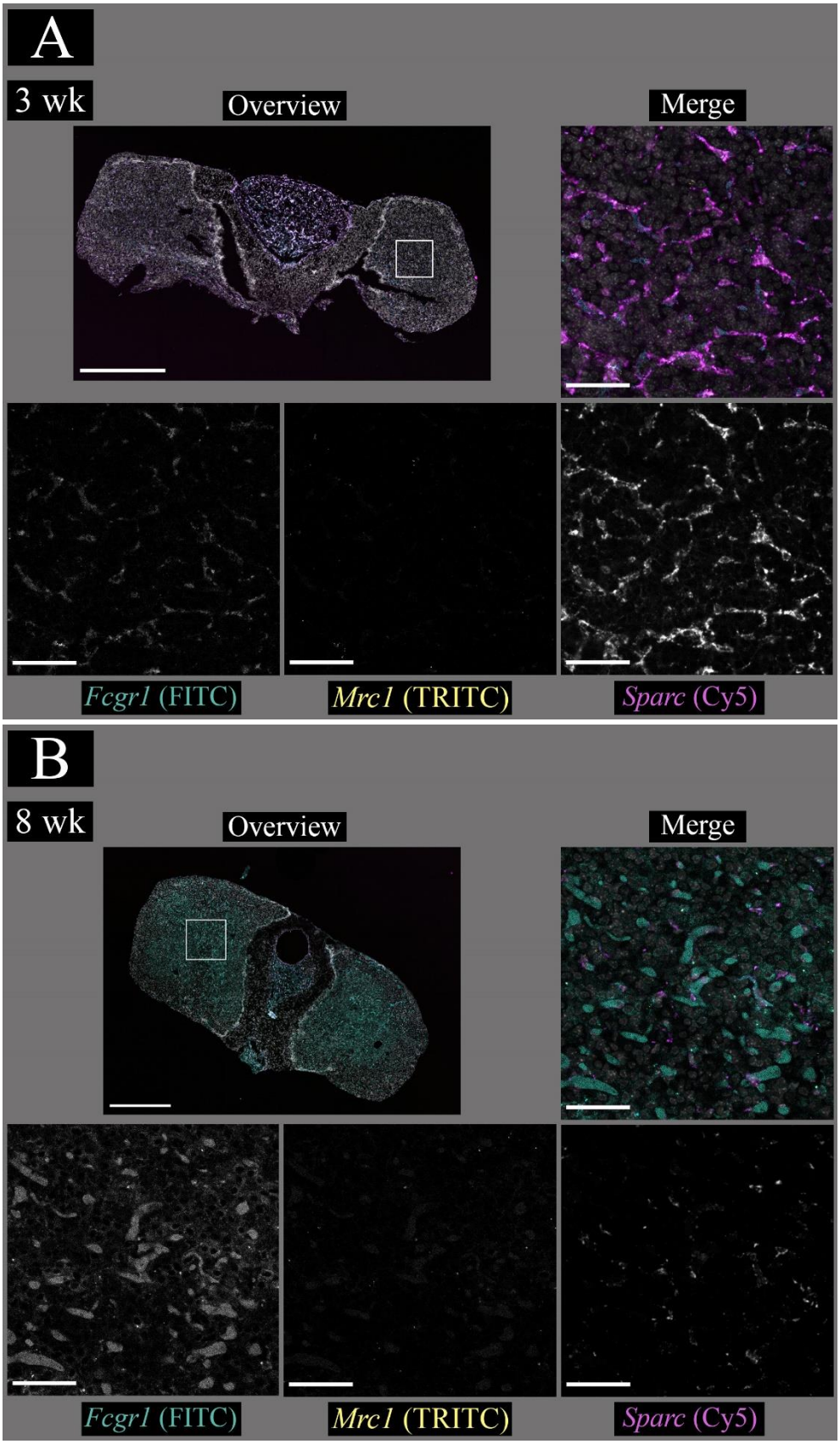

Figure 9. Pituitary sections from (A) a 3-week-old C57BL/6NRj mouse and (B) an 8-week-old C57BL/6NRj mouse from the 3rd staining experiment. The scale bar in the overview images is 400 µm and in the close-ups, from the regions of interest, 50 µm. The colour of the targets in the overview and merge images are specified by the colours of the target name. The signal from nuclei is in grayscale in the overview and merge images.

3.2 Immunofluorescence staining results

The first intent was to detect EFG-like module-containing mucin-like hormone receptor-like 1 (F4/80) with the four target hormones, GH, LH, PRL and TSH. F4/80 was targeted first with a conjugated antibody but it did not give any specific signal. Concentration of the antibody was increased, and later, unconjugated antibodies were tested. None of the staining methods gave any specific signal from F4/80, so it was excluded and only the four hormones were targeted in the following staining along with nuclei with DAPI stain. Every target hormone gave a clear specific signal alongside nuclei (Figures 10-13).

First, secreted growth hormone (GH) was visualized from the pituitaries of 5 week old mice. The GH signal in the anterior lobe seemed to be evenly spread so that no visible clusters appeared inside the area (Figure 10). GH signal was a bit clearer in the knock-out pituitaries than in the wild-type ones so at first the signal seemed to be more frequent in the wild-types than in the knock-outs.

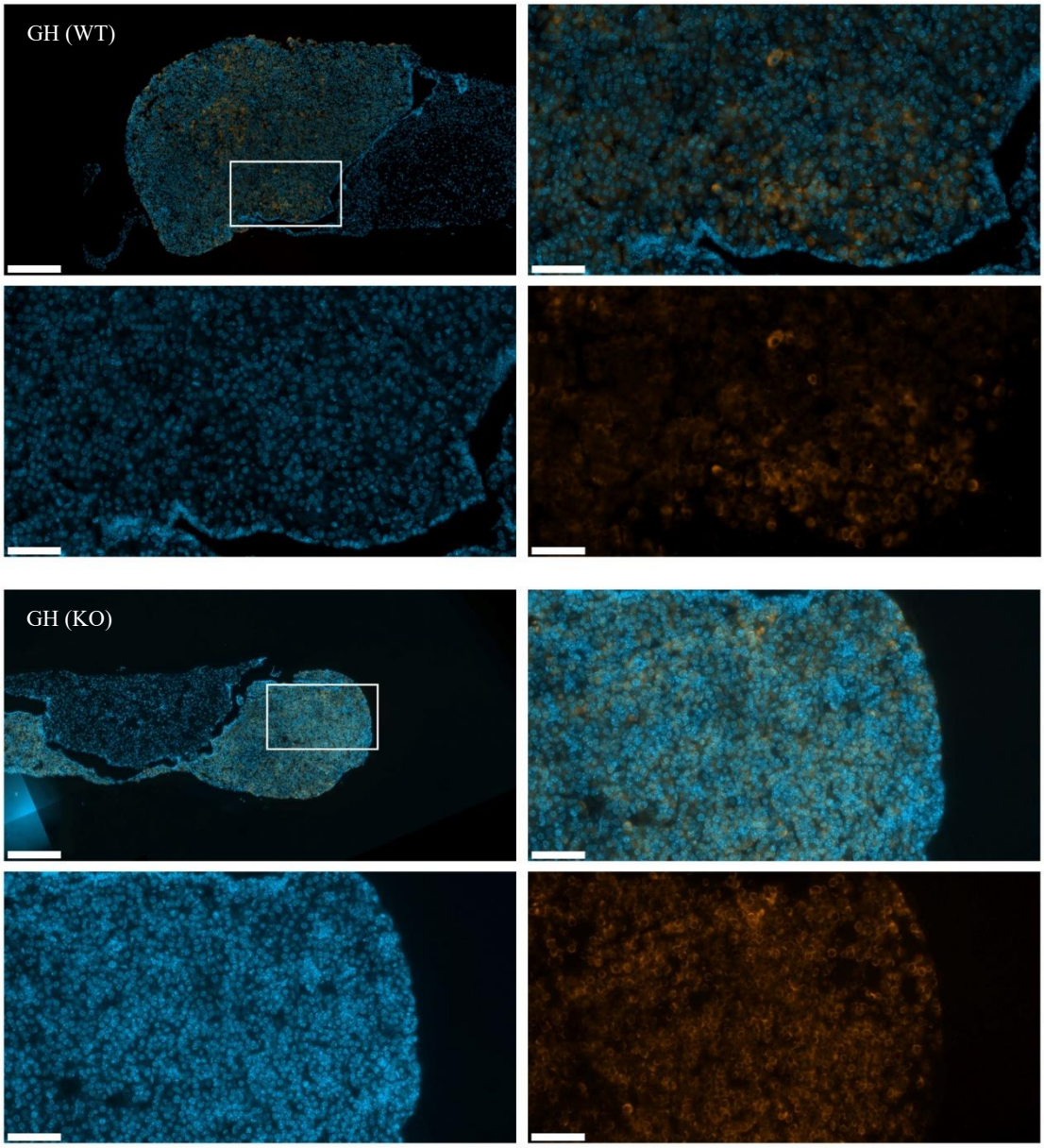

Figure 10. Overview and close-up images of the stained pituitary gland from a wild-type (WT) and a Plvap$^{-/-}$ (KO) mouse taken with Pannoramic Midi fluorescence slide scanner. Signals can be seen from nuclei (turquoise) and secreted GH (orange). In the upper close-up images, the two signals are merged while the lower images show close-ups from the signals separately. Scale bar in the overview images is 100 µm and in close-ups, from the regions of interest, 20 µm.

Secreted luteinizing hormone (LH) was also visualized from the 5-week-old mouse pituitaries. From both wild-type and knock-out mice, a clear signal from LH could be seen (Figure 11). More signal appeared in the wild-type border area of the anterior pituitary section, while in the knock-out pituitary, the localization was not as clear. The amount of hormonal cell signal from the whole area seemed at first to be similar between the two mouse strains.

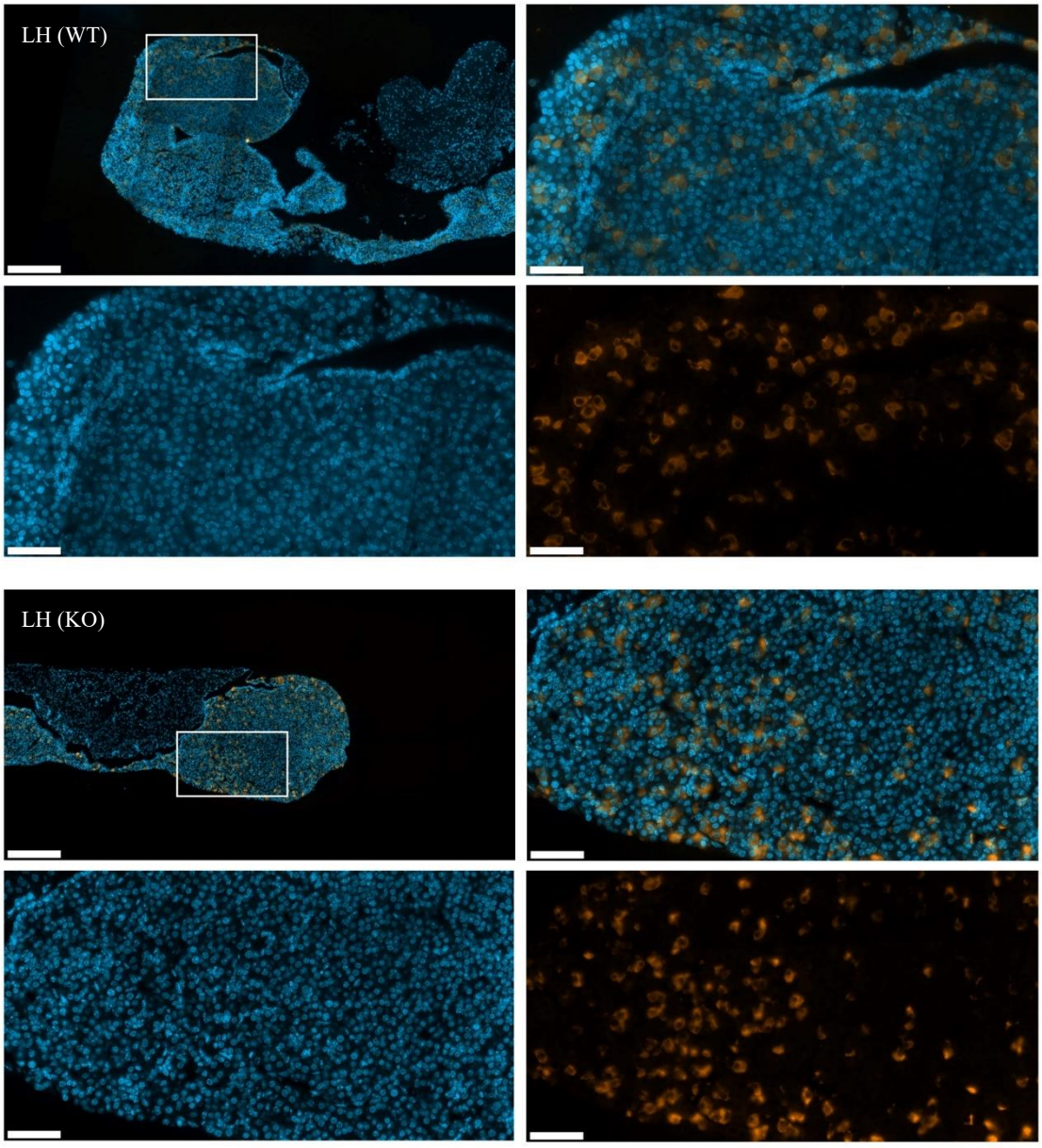

Figure 11. Overview and close-up images of the stained pituitary gland from a wild-type (WT) and a Plvap$^{-/-}$ (KO) mouse taken with Pannoramic Midi fluorescence slide scanner. Signals can be seen from nuclei (turquoise) and secreted LH (orange). In the upper close-up images, the two signals are merged while the lower imagess show close-ups from the signals separately. Scale bar in the overview images is 100 µm and in close-ups, from the regions of interest, 20 µm.

From the 5-week-old mouse pituitaries, the secreted prolactin (PRL) was visualized but the wild-type signal is fainter than the knock-out signal (Figure 12). As the wild-type nuclei signal is faint as well, the staining simply seemed not to work as well for the wild-type sample. No specific signal localization or significant differences in the number of positive hormonal cells could be seen between the different mouse strains.

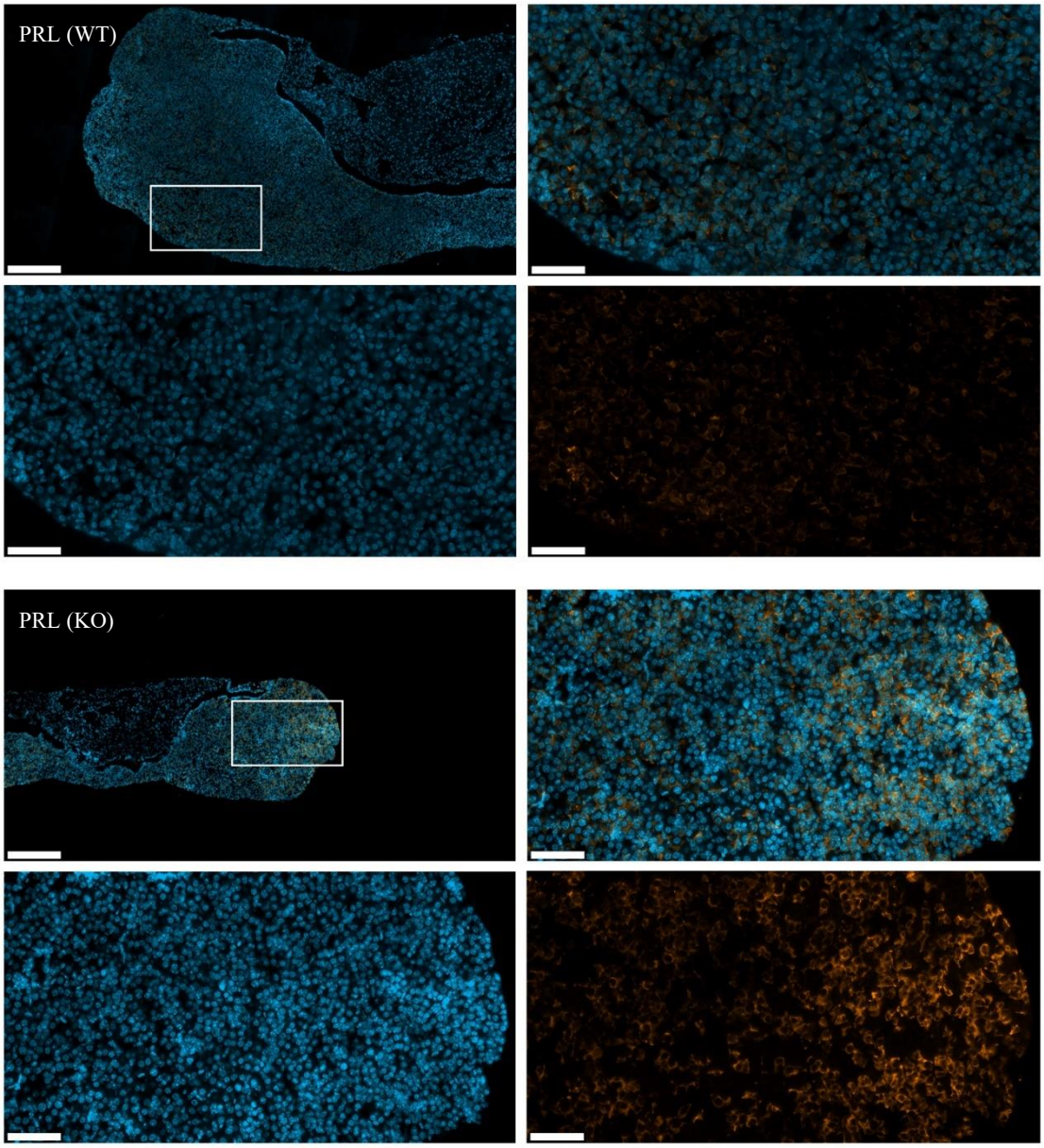

Figure 12. Overview and close-up images of the stained pituitary gland from a wild-type (WT) and a Plvap$^{-/-}$ (KO) mouse taken with Pannoramic Midi fluorescence slide scanner. Signals can be seen from nuclei (turquoise) and secreted PRL (orange). In the upper close-up images, the two signals are merged while the lower images show close-ups from the signals separately. Scale bar in the overview images is 100 µm and in close-ups, from the regions of interest, 20 µm.

Last, secreted thyroid-stimulating hormone (TSH) signal could be seen clearly in both wild-type and knock-out pituitaries (Figure 13). The signals were evenly spread in the anterior part of the pituitary gland. Comparing to signals from other secreted hormones, TSH seemed to be the most infrequent. It also looked as if the wild-type pituitary does not have as many TSH secreting cells than the knock-out pituitary.

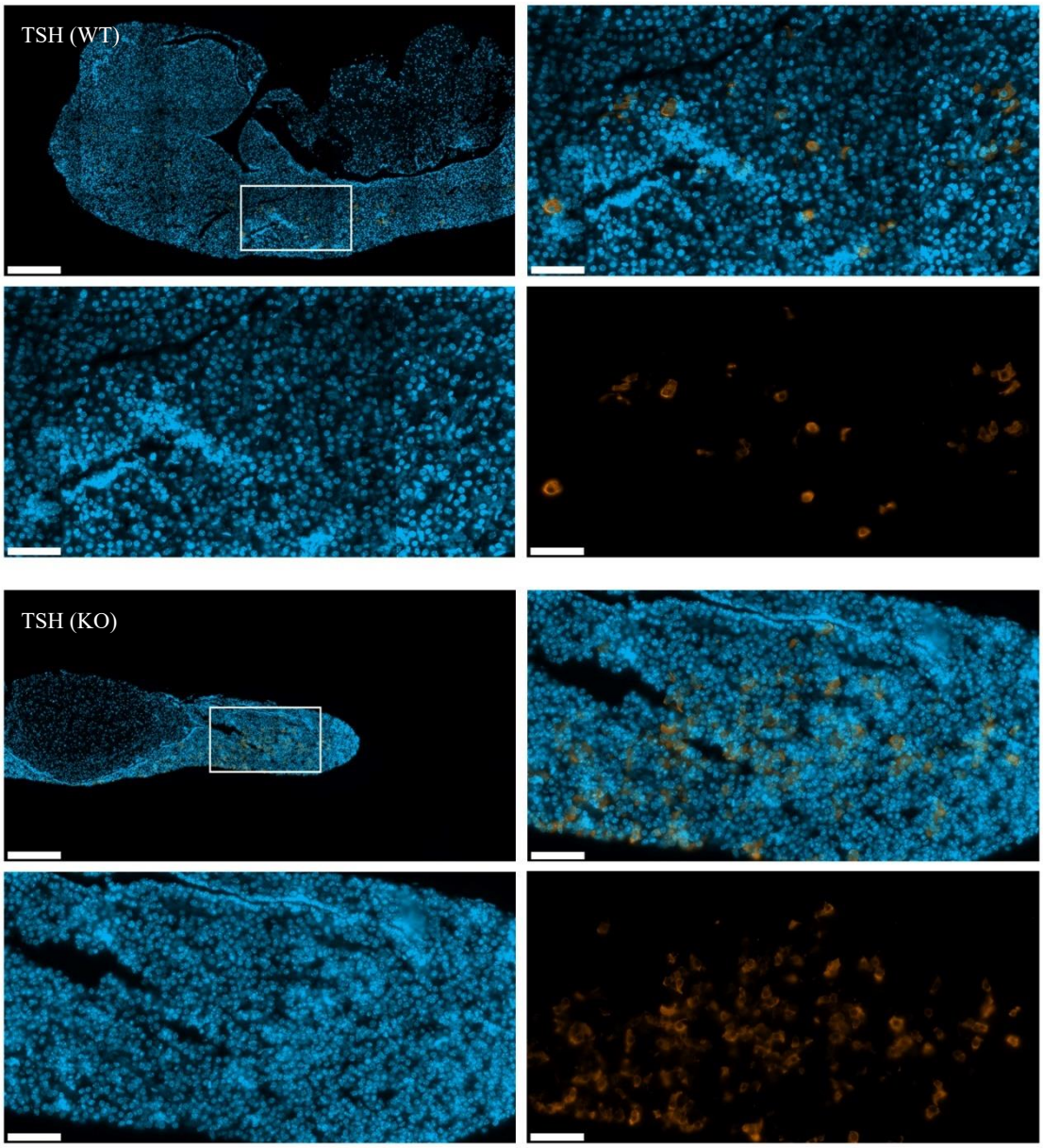

Figure 13. Overview and close-up images of the stained pituitary gland from a wild-type (WT) and a Plvap$^{-/-}$ (KO) mouse taken with Pannoramic Midi fluorescence slide scanner. Signals can be seen from nuclei (turquoise) and secreted TSH (orange). In upper close-up images the two signals are merged while the lower images show close-ups from the signals separately. Scale bar in the overview images is 100 µm and in close-ups, from the regions of interest, 20 µm.

Active hormonal cells were counted manually from total of six pituitary sections per target hormone from three wild-type and three knock-out individuals. To get the total amount of positive hormone-releasing cells per pituitary, positive hormonal signals were counted from half of the entire pituitary section and the value was multiplied by two. Quantification of the cells showed that the number of positive cells secreting GH and LH were significantly lower in the pituitary of the knock-out mice than in the wild-type mice (Figure 14). Accordingly, the number of positive hormonal cells secreting PRL and TSH showed no significant differences between the two mouse strains.

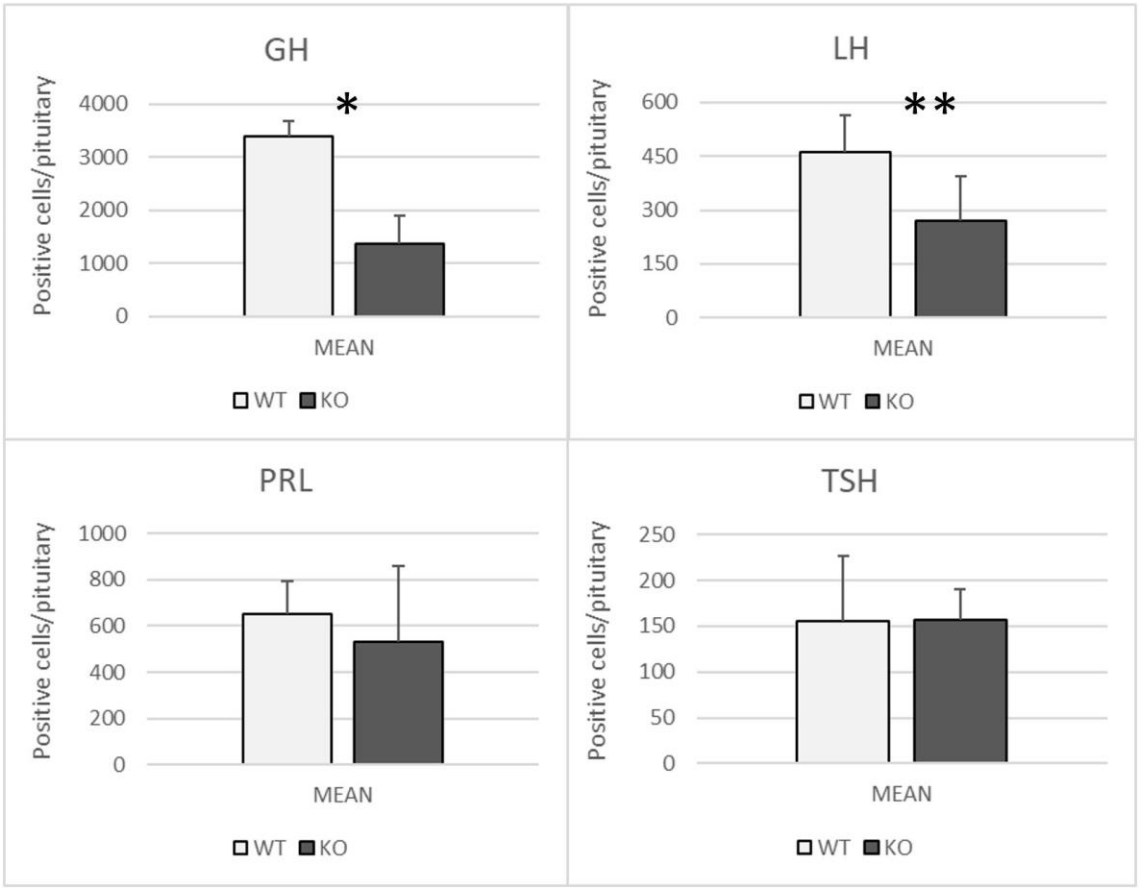

Figure 14. Quantification of the number of positive hormone-releasing cells in the posterior lobe of the pituitary in 5-week-old mice (mean + standard deviation). The number of positive cells of growth hormone (GH) and luteinizing hormone (LH) is significantly higher in the wild-type (WT) mice (n = 6) than in the knock-out (KO) mice (n = 6) (*$p < 0.05$, **$p < 0{,}0001$). The number of hormonal cells secreting prolactin (PRL) and thyroid-stimulating hormone (TSH) in the pituitary are not significantly different between the two mouse strains.

3.3 Haematoxylin & eosin staining results

Haematoxylin & eosin staining protocol was first tested with only wild-type pituitary samples. Staining resulted the tissue sections to be rather pink so the eosin incubation time was dropped from 45 seconds to 30 seconds. Incubation decrease gave satisfying colorization. After staining and imaging, it could be seen that in some of the pituitary sections the posterior lobe was not clearly visible meaning that the pituitary paraffin blocks were not cut deep enough, or in contrast, they were cut too deep (Figures 15). Also, some of the tissue sections were broken. Different cell types could be recognized from the images: acidophils, basophils and chromophobes. These cells are marked by arrows in Figure 21A. Acidophils in the anterior pituitary gland secrete GH and PRL and stain pink. Basophils secrete TSH and LH and typically stain deep blue or purple. Chromophobes on the other hand do not stain well and they appear pale. Some arteries with blood cells were also easily recognizable for example in Figure 15B in the middle close-up image. No histological differences could be spotted from the pituitary sections when comparing CCR2$^{-/-}$ (Figure 15B) and Nur77$^{-/-}$ mice (Figure 15C) with the wild-types (Figure 15A). The knock-outs had all the different cell types as the wild-type pituitaries had and the blood vessels looked normal as well.

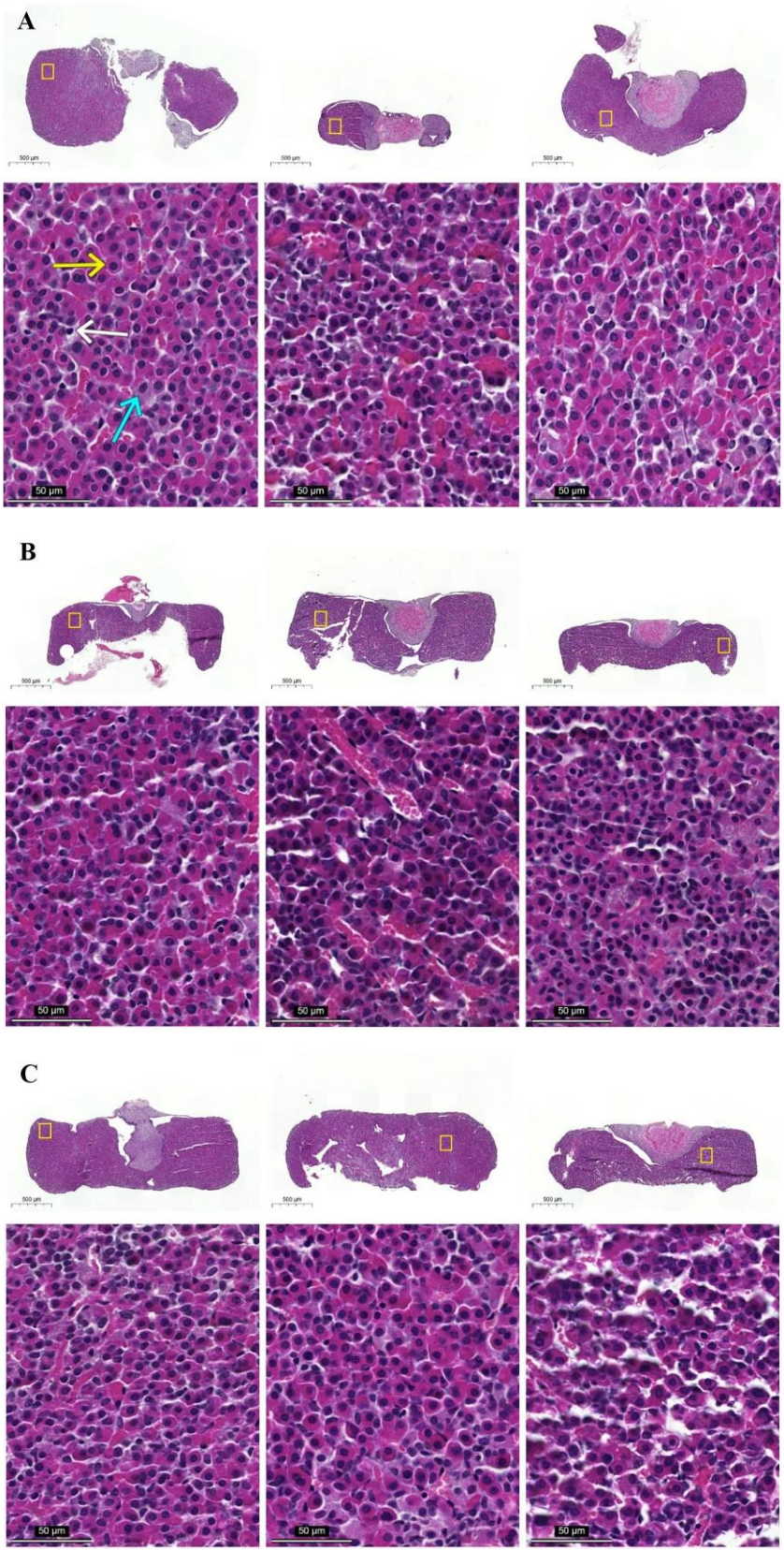

Figure 15. Haematoxylin- and eosin-stained formalin- and PFA-fixed pituitary sections from (A) C57BL/6NRj, (B) CCR2 knock-out and (C) Nur77 knock-out mice individuals. Regions of interest (in yellow) are beneath the overview sections. In (B) and (C) the left pituitary is formalin-fixed; two other pituitaries in the middle and right are PFA-fixed. Acidophils (the yellow arrow in A), chromophobes (the white arrow in A) and basophils (the turquoise arrow in A) can be recognized from the close-up images.

4 DISCUSSION

4.1 RNAscope® and immunofluorescence staining

RNAscope® assay was used to study macrophage populations in the anterior pituitary gland by detecting macrophage-specific gene expression. Based on the results, I could not identify different macrophage populations nor learn how they change during age. Other studies have shown that in rat both the anterior and the posterior lobe have macrophages while the intermediate lobe has few (Mander & Morris 1996, Yagasaki et al. 2021). This indicates that the RNAscope® method was not suitable for this macrophage study. Some probe signals could be obtained in the experiments but it was unclear if the signals came specifically from macrophages as the signal from *Fcgr1* was not properly detected. Contradictory results were obtained from *Sparc* as well as the target gave signal from the same spots than *Fcgr1* but earlier unpublished studies have shown that few macrophages express *Sparc*.

To further study the localization of the macrophages while simultaneously detecting the hormone-releasing cells in the pituitary, immunofluorescence staining was done for wild-type mice and a knock-out strain. Since F4/80, a glycoprotein appearing in the cell surface of macrophages, could not be detected, only hormonal activities could be studied. This means it was not possible to investigate if colocalization happens between macrophages and the hormone-releasing cells. There are no previous immunofluorescence staining studies targeting both active hormonal cells and macrophages even though macrophages have been detected using F4/80 antibody (Sun et al. 2015, Wang et al. 2019). Still, the study shows significant differences in the hormone-releasing cell numbers between wild-type and knock-out mice. For future studies the detection of both F4/80 and the hormonal cells would be good to achieve. The third staining experiment in this study had the same incubation times Wang et al. (2019) had for the primary and secondary antibodies in their study. Using exactly the same antibodies as Wang et al. (2019) or Sun et al. (2015) could be worth trying.

Based on an unpublished data from Rantakari research group, a decrease of some of the hormone-releasing cells was to be expected in the pituitary of Plvap$^{-/-}$ mice, which lack the fetal liver-derived macrophages. Only the numbers of hormone-releasing cells secreting growth hormone (GH) and luteinizing hormone (LH) were significantly lower

in the knock-out strain than in the wild-types. This result shows that macrophages originating from the fetal liver seem to affect the secretory cells of GH and LH. The number of hormonal cells secreting prolactin (PRL) and thyroid-stimulating hormone was not significantly different. Hormonal measurements from Plvap$^{-/-}$ mice have shown that in the bloodstream and the pituitary tissue PRL levels are low (unpublished data from Rantakari research group). However, this study gives clear evidence that there are active hormonal cells producing PRL in the anterior lobe of the pituitary. The hormone might get stored somewhere else but production still takes place in the pituitary.

The pituitary of Plvap$^{-/-}$ mice is smaller than in wild-type mice. The area was first regarded but then left unconsidered because it seemed to distort the results. It could still be good to think about the impact the pituitary area has when comparing number of certain cells. It is hard to say if the cells are the same size or smaller in the knock-outs than in the wild-type pituitary. At least, when comparing the study images, they seem to be more packed in the knock-out pituitary. The size of the cells and the area might affect the number of the hormonal cells.

4.2 Histological comparison using haematoxylin and eosin staining

Along with the abovementioned experiments haematoxylin and eosin staining of the pituitary was included in the study. If there would be any histological differences in the anterior pituitary gland of two knock-out mouse models and wild-type mice, it could give an insight into the impact macrophages have on the hormone-releasing cells. However, no visible differences could be found when the final images between the mouse strains were compared. All pituitary samples seemed to have approximately the same amount of acidophils, basophils and chromophobes, and no specific localization occurred among the cells. This means that even though the Nur77$^{-/-}$ knock-out mouse model lacks Ly6C^{low} monocytes and the other knock-out CCR2 protein, which is involved in macrophage recruitment, the changed macrophage populations do not seem to affect the colonization or the number of the hormone-releasing cells in the anterior part of the pituitary.

4.3 Technical problems

All in all, the pituitary gland itself seemed to cause trouble due to its small size. It is difficult to remove without damaging the structure of the gland. Some residues from other parts of the brain can go unnoticed along with the pituitary to the paraffin block. The size

is challenging also during the microtome cutting as the organ tears easily. Some of the protocol steps can be too rough for the cut pituitary sections. For example, after boiling the tissue slides during the RNAscope® method, some of the sections were missing: In all the staining sets some of the 1-week sections got boiled away and in the first set one newborn section as well. This sets a challenge to get good tissue sections for imaging and examination.

The RNAscope® method did not give the best results with the pituitary tissue sections. The idea at first was to detect every target signal at once, but the Texas Red channel with Opal™ 620 fluorophore was impossible to image together with Opal™ 570 fluorophore (TRITC) so adjustments had to be made. Some of the signal strength differences in the overview images and close-ups were mostly due to the sudden microscope change and hence different set-ups. LSM880 microscope was used to image the rest of the sample slides because there came an unexpected problem in LSM780 with detecting nuclei in the DAPI channel.

Since there seemed to be a lot of autofluorescence especially with Opal™ 520 fluorophore in FITC channel an autofluorescence quenching procedure was added to the RNAscope® assay. Consequently, ProLong™ Gold mounting medium was replaced by the kit's medium, VECTASHIELD®, because it gave clearer images. The autofluorescence kit did improve the image quality and was easy to use. The images still showed some autofluorescence signal but since the target probe signals were faint the background came more visible when the target signal was enhanced.

The RNAscope® staining did not always work for all the target probes, making the technique unreliable. Some of the positive control images don't show any specific signals so the blank target images do not show any signal either. The wide range in signal strengths was challenging for the editing process of the images. Some of the target signals were so strong that with the same settings there might not be any visible signal left in the control image. This was the case also with some strong positive control signal and with faint target signal.

The immunofluorescence experiment did not go as first was planned because signal from F4/80 could not be attained. The conjugated antibody concentration was first increased and since it did not improve the results, a primary and a secondary antibody was tested

next. Changing the antibody did not help and the lack of signal remains unknown. There might have been a problem with the antibodies themselves or something might have gone wrong with the protocol. The final experiment slides were imaged first with ZEISS LSM880 confocal microscope and then with Pannoramic Midi fluorescence slide scanner. The slide scanner was slower to use but the quality of the images was much better than with LSM880. Good quality naturally helped the counting of the cells. Still, it is important to value the counting itself. Since signal strength was not considered, only cells that showed any signal clearly around the nucleus were counted. There were hundreds and even thousands of cells to count manually and it was occasionally hard to decide whether a signal was good enough to be counted or not. The error bars show variety in the results that might have resulted from counting errors. Another consideration is the depth of the pituitary tissue sections. Natural variation might occur in the number of hormone-releasing cells depending on where the section in question is taken from the pituitary.

5 CONCLUSIONS

The RNAscope® method did not give any reliable results of macrophage populations in the pituitary gland nor from their localization in the anterior lobe. Some positive probe activity could be detected but it was unclear whether it was from macrophages or from other cells. The number of hormone-releasing cells secreting prolactin and thyroid-stimulating hormone was not significantly different between in the Plvap knock-out mice when compared to wild-type mice. The high prolactin secreting cell number was unexpected since earlier unpublished study has measured a low amount of prolactin in the pituitary gland. In contrast, significant decrease in the number of hormonal cells secreting growth hormone and luteinizing hormone could be seen in the Plvap$^{-/-}$ mice when compared to wild-type mice. This suggests that the fetal liver-derived macrophages have an effect on the secretory cells of growth hormone and luteinizing hormone while monocyte derived macrophages do not affect those cells. Histological comparison of the pituitary tissue sections of Nur77 and CCR2 knock-out mice to wild-type mice showed no differences.

In the future, it would be interesting to study the prolactin secretion further in the Plvap mouse model. Now it remains unknown why the hormonal measurements gave a low prolactin level as a result while in this study the results clearly show that there are as much hormonal cells producing prolactin as there is in the wild-type mice. The impact fetal liver-derived macrophages have on the hormone-releasing cells needs to be studied more as well. Thus, getting F4/80 represented at the same time with hormone-releasing cells would be beneficial to get information from the macrophages. Also, another more suitable method could replace the RNAscope® assay to get proper detection of the designated genes in this study and therefore, more information could be obtained from the macrophage populations in the pituitary.

6 REFERENCES

Asa S. 2007. Pituitary Histopathology in Man: Normal and Abnormal. In: Feingold KR, Anawalt B, Boyce A, Chrousos G, de Herder W, Dhatariya K, Dungan K, Grossman A, Hershman JM, Hofland J, Kalra S, Kaltsas G, Koch C, Kopp P, Korbonits M, Kovacs CS, Kuohung W, Laferrère B, McGee E, McLachlan R, Morley J, New M, Purnell J, Sahay R, Singer F, Stratakis C, Trence D, Wilson D. (editors). *Endotext*. South Dartmouth (MA): MDText.com, Inc.; 2000-, PMID: 25905234.

A-Gonzalez N. & Castrillo A. 2018. Origin and specialization of splenic macrophages. *Cellular Immunology* 330, 151-158.

Backer R, Schwandt T, Greuter M, Oosting M, Jungerkes F, Tuting T, Boon L, O'Toole T, Kraal G, Limmer A. and den Haan J. 2010. Effective collaboration between marginal metallophilic macrophages and CD8+ dendritic cells in the generation of cytotoxic T cells. *Proceedings of the National Academy of Sciences* 107, 216-221.

Beattie L, Sawtell A, Mann J, Frame T, Teal B, de Labastida Rivera F, Brown N, Walwyn-Brown K, Moore J, MacDonald S, Lim E-K, Dalton J, Engwerda C, MacDonald K. and Kaye P. 2016. Bone marrow-derived and resident liver macrophages display unique transcriptomic signatures but similar biological functions. *Journal of Hepatology* 4, 758-768.

Brestoff J, Wilen C, Moley J, Li Y, Zou W, Malvin N, Rowen M, Saunders B, Ma H, Mack M, Hykes B. Jr, Balce D, Orvedahl A, Williams J, Rohatgi N, Wang X, McAllaster M, Handley S, Kim B, Doench J, Zinselmeyer B, Diamond M, Virgin H, Gelman A. and Teitelbaum S. 2021. Intercellular mitochondria transfer to macrophages regulates white adipose tissue homeostasis and is impaired in obesity. *Cell Metabolism* 2, 270-282.

Calandra T. & Roger T. 2003. Macrophage migration inhibitory factor: a regulator of innate immunity. *Nature Reviews Immunology* 3, 791-800.

Cox N. & Geissmann F. 2020. Macrophage ontogeny in the control of adipose tissue biology. *Current Opinion in Immunology* 62, 1-8.

Duffield J. 2003. The inflammatory macrophage: a story of Jekyll and Hyde. *Clinical Science* 104, 27-38.

Duffield J, Forbes S, Constandinou C, Clay S, Partolina M, Vuthoori S, Wu S, Lang R. and Iredale J. 2005. Selective depletion of macrophages reveals distinct, opposing roles during liver injury and repair. *The Journal of Clinical Investigation* 115, 56-65.

Fantin A, Vieira J, Gestri G, Denti L, Schwarz Q, Prykhozhij S, Peri F, Wilson S. and Ruhrberg C. 2010. Tissue macrophages act as cellular chaperones for vascular anastomosis downstream of VEGF-mediated endothelial tip cell induction. *Blood* 116, 829-840.

Fonseca R, Bassi G, Brito C, Rosa L, David B, Araújo A, Nóbrega N, Diniz A, Jesus I, Barcelos L, Fontes M, Bonaventura D, Kanashiro A, Cunha T, Guatimosim S, Cardoso V, Fernandes S, Menezes G, Lartigue G. and Oliveira A. 2019. Vagus nerve regulates the phagocytic and secretory activity of resident macrophages in the liver. *Brain, Behavior, and Immunity* 81, 444-454.

Fujiwara K, Yatabe M, Tofrizal A, Jindatip D, Yashiro T and Nagai R. 2017. Identification of M2 macrophages in anterior pituitary glands of normal rats and rats with estrogen-induced prolactinoma. *Cell and Tissue Research* 368, 371-378.

Ginhoux F. & Guilliams M. 2016. Tissue-resident macrophage ontogeny and homeostasis. *Immunity* 44, 439-449.

Guilliams M. & Scott C. 2017. Does niche competition determine the origin of tissue-resident macrophages? *Nature Reviews Immunology* 17, 451-460.

Hagan C, Bolon B. and Dirk C. 2012. *Comparative anatomy and histology; A mouse and human atlas*, 343-384.

Han C, Juncadella I, Kinchen J, Buckley M, Klibanov A, Dryden K, Onengut-Gumuscu S, Erdbrügger U, Turner S, Shim Y, Tung K. and Ravichandran K. 2016. Macrophages redirect phagocytosis by non-professional phagocytes and influence inflammation. *Nature* 539, 570-574.

Hoeffel G. & Ginhoux F. 2018 Fetal monocytes and the origins of tissue-resident macrophages. *Cellular Immunology* 330, 5-15.

Hulsmans M, Clauss S, Xiao L, Aguirre A, King K, Hanley A, Hucker W, Wülfers E, Seemann G, Courties G, Iwamoto Y, Sun Y, Savol A, Sager H, Lavine K, Fishbein G, Capen D, Da Silva N, Miquerol L, Hiroko H, Seidman C, Seidman J, Sadreyev R, Naxerova K, Mitchell R, Brown D, Libby P, Weissleder R, Swirski F, Kohl P, Vinegoni C, Milan D, Ellinor P. and Nahrendorf M. 2017. Macrophages facilitate electrical conduction in the heart. *Cell* 169, 510-522.

Jones R. & Lopez K. 2015. *Human Reproductive Biology*, 4th edition, 3-22.

Knutson M, Oukka M, Koss L, Aydemir F. and Wessling-Resnick M. 2005. Iron release from macrophages after erythrophagocytosis is up-regulated by ferroportin 1 overexpression and down-regulated by hepcidin. *Proceedings of the National Academy of Sciences* 102, 1324-1328.

Kraal G. 1992. Cells in the marginal zone of the spleen. *International Review of Cytology* 132, 31-74.

Krenkel O. & Tacke F. 2017. Liver macrophages in tissue homeostasis and disease. *Nature Reviews Immunology* 17, 306-321

Lahaye C, Gladine C, Pereira B, Berger J, Chinetti-Gbaguidi G, Lainé F, Mazur A. and Ruivard M. 2021. Does iron overload in metabolic syndrome affect macrophage profile? A case control study. *Journal of Trace Elements in Medicine and Biology* 67, 126786.

Lavin Y, Winter D, Blecher-Gonen R, David E, Keren-Shaul H, Merad M, Jung S. and Amit I. 2014. Tissue-resident macrophage enhancer landscapes are shaped by the local microenvironment. *Cell* 159, 1312-1326.

Liu C, Yang X, Wu J, Kuei C, Mani N, Zhang L, Yu J, Sutton S, Qin N, Banie H, Karlsson L, Sun S. and Lovenberg T. 2014. Oxysterols direct B-cell migration through EBI2. *Nature* 475, 519-523.

Mander T. & Morris J. 1996. Development of microglia and macrophages in the postnatal rat pituitary. *Cell and Tissue Research* 286**,** 347-355.

Maronpot R. & Brix A. 2014. Cited 5.5.2021
https://ntp.niehs.nih.gov/nnl/endocrine/pituitary/index.htm

Marques P, Barry S, Carlsen E, Collier D, Ronaldson A, Awad S, Dorward N, Grieve J, Mendoza N, Muquit S, Grossman A, Balkwill F. and Korbonits M. 2019. Chemokines modulate the tumour microenvironment in pituitary neuroendocrine tumours. *Acta Neuropathologica Communications* 7, 172.

Martin P. & Gurevich D. 2021. Macrophage regulation of angiogenesis in health and disease. *Seminars in Cell & Developmental Biology* 119, 101-110.

Martinez-Pomares L. & Gordon S. 2020. Macrophages and Autoimmunity. *The Autoimmune Diseases,* 6th edition, 191-212.

Muñoz-Espín D, Cañamero M, Maraver A, Gómez-López G, Contreras J, Murillo-Cuesta S, Rodríguez-Baeza A, Varela-Nieto I, Ruberte J, Collado M. and Serrano M. 2013. Programmed cell senescence during mammalian embryonic development. *Cell* 155, 1104-1118.

Nash A, Dalziel R. and Fitzgerald R. 2015. The Immune Response to Infection. *Mims' Pathogenesis of Infectious Disease*, 6th edition, 119-144.

Nolte M, Arens R, Kraus M, van Oers M, Kraal G, van Lier R. and Mebius R. 2004. B cells are crucial for both development and maintenance of the splenic marginal zone. *The Journal of Immunology* 6, 3620-3627.

Recalcati S, Locati M, Gammella E, Invernizzi P. and Cairo G. 2012. Iron levels in polarized macrophages: Regulation of immunity and autoimmunity. *Autoimmunity Reviews* 11, 883-889.

Schindelin J, Arganda-Carreras I, Frise E, Kaynig V, Longair M, Pietzsch T, Preibisch S, Rueden C, Saalfeld S, Schmid B, Tinevez J-V, White D, Hartenstein V, Eliceiri K, Tomancak P. and Cardona A. 2012. Fiji: an open-source platform for biological-image analysis. *Nature Methods* 9, 676-682.

Simões F, Cahill T, Kenyon A, Gavriouchkina D, Vieira J, Sun X, Pezzolla D, Ravaud C, Masmanian E, Weinberger M, Mayes S, Lemieux M, Barnette D, Gunadasa-Rohling M, Williams R, Greaves D, Trinh L, Fraser S, Dallas S, Choudhury R, Sauka-Spengler T. and Riley P. 2020. Macrophages directly contribute collagen to scar formation during zebrafish heart regeneration and mouse heart repair. *Nature Communications* 11, 600.

Sun X, Gao D, Gao L, Zhang C, Yu X, Jia B, Wang F. and Liu Z. 2015. Molecular imaging of tumor-infiltrating macrophages in a preclinical mouse model of breast cancer. *Theranostics* 5, 597-608.

Takahashi M, Misaki M, Shibata S, Iga T, Shindo T, Tai-Nagara I, Hirata A, Ogawa M, Miyamoto T, Nakagawa T, Ema M, Ichiyama Y, Shima D, Hozumi K, Nishimura S. and Kubota Y. 2020. Macrophages fine-tune pupil shape during development. *Developmental Biology* 464, 137-144.

Toews G. 2009. Macrophages. *Asthma and COPD,* 2nd edition, 133-143.

T'Jonck W, Guilliams M. and Bonnardel J. 2018. Niche signals and transcription factors involved in tissue-resident macrophage development. *Cellular Immunology* 330, 43-53.

Wang Q, Xin Z, Yang L, Luo M, Han L, Lu Y, Shi Q, Wang Y. and Liang Q. 2019. Gentiopicroside (GENT) protects against sepsis induced by lipopolysaccharide (LPS) through the NF-κB signaling pathway. *Annals of Translational Medicine* 7, 731-731.

Wilkinson H, Roberts E, Stafford A, Banyard K, Matteucci P, Mace K. and Hardman M. 2019. Tissue iron promotes wound repair via M2 macrophage polarization and the chemokine (C-C Motif) ligands 17 and 22. *The American Journal of Pathology* 189, 2196-2208.

Wolf Y, Boura-Halfon S, Cortese N, Haimon Z, Sar Shalom H, Kuperman Y, Kalchenko V, Brandis A, David E, Segal-Hayoun Y, Chappell-Maor L, Yaron A. and Jung S. 2017. Brown-adipose-tissue macrophages control tissue innervation and homeostatic energy expenditure. *Nature Immunology* 18, 665-674.

Yagasaki Y, Katayama Y, Kinoshita Y, Nagata T, Kawakami Y. and Miyata M. 2021. Macrophages are activated in the rat anterior pituitary under chronic inflammatory conditions. *Neuroscience Letters* 748, 135688.

Zhao W, Zhang Y, Ji R, Knight G, Burnstock G, Yuan H. and Xiang Z. 2020. Expression of P2X receptors in the rat anterior pituitary. *Purinergic signalling* 1, 17-28.

APPENDIXES

1. RNAscope® Multiplex Fluorescent Reagent Kit v2 assay protocol (modified after ACDBio)

Important procedural guidelines

- Use only samples mounted on SuperFrost® Plus Slides (Fisher Scientific)
- Always run positive and negative control probes on your sample to assess sample RNA quality and optimal permeabilization.

FFPE sample preparation and pre-treatment

1. Immediately following dissection, fix tissue in 10 % normally buffered formalin for 16-32 h at RT. Fixation time will vary depending on tissue type and size.
2. Wash sample with 1X PBS.
3. Dehydrate sample using a standard ethanol series (50 % EtOH 30 min, 70 % EtOH 1 h, store in fresh 70 % EtOH.
4. Embedding in paraffin.
5. Trim paraffin blocks as needed and cut embedded tissue into 5 +/– 1 µm sections using a microtome.
6. Place paraffin ribbon in a 40-45 °C water bath, and mount sections on SuperFrost® Plus slides. Place tissue in the center of the slide.
7. Air dry slides overnight at RT.
8. Bake slides in a dry oven (HybEZ™ Oven) for 1 h at 60 °C.
9. Deparaffinize FFPE sections in fume hood (agitate the slides by occasionally lifting the slide rack up and down in the dish).
    a. Xylene 2 x 5 min.
    b. EtOH 100 % 2 x 2 min.
10. Remove the slides from the rack, and place on absorbent paper with the section face-up. Dry slides for 5 min. at RT (or until completely dry).

Prepare HybEZ™ Oven and RNAscope® 1X Target Retrieval Reagents

1. Turn on the HybEZ™ Oven and set the temperature to 40 °C.
2. Place a humidifying paper in the Humidity Control Tray and wet completely with dH_2O.

3. Insert the covered tray into the oven and close the oven door. Warm the tray for 30 min. at 40°C before use. Keep the tray in the oven when not in use.
4. Prepare 700 ml of fresh RNAscope® 1X Target Retrieval Reagents by adding 630 ml distilled water to 1 bottle (70 ml) 10X Target Retrieval Reagents in the beaker. Mix well.

Pre-treat 1: Apply RNAscope® Hydrogen Peroxide

1. Lay the deparaffinized slides on the bench and add ~5-8 drops of RNAscope® Hydrogen Peroxide (H_2O_2) to cover each section.
2. Incubate slides for 10 min. at RT.
3. Remove RNAscope® Hydrogen Peroxide solution from one slide at a time by tapping and/or flicking the slide on absorbent paper. Immediately insert the slide into a Slide Rack submerged in a Staining Dish filled with distilled water.
4. Wash slides twice by moving the Slide Rack up and down in dH_2O.

Pre-treat 2: Perform manual target retrieval

1. Place the beaker containing RNAscope® 1X Target Retrieval Reagents on the hot plate. Cover the beaker with foil and turn the hot plate on high for 10-15 min. IMPORTANT! Do not boil the 1X RNAscope® Target Retrieval Reagents more than 15 min. before use.
2. Once 1X RNAscope® Target Retrieval Reagents reaches a mild boil (98-102 °C), turn the hot plate to a lower setting to maintain the correct temperature. Check the temperature with a thermometer.
3. With a pair of long forceps very slowly submerge the slide rack containing the slides into the mildly boiling RNAscope® 1X Target Retrieval Reagents solution. Cover the beaker with foil and boil the slides for 15 min.
4. Use the forceps to immediately transfer the hot slide rack from the RNAscope® 1X Target Retrieval Reagents to the staining dish containing distilled water. Do not let the slides cool in the Target Retrieval Reagents solution.
5. Wash slides by moving the Slide Rack up and down in dH_2O.
6. Wash the slides with fresh 100 % alcohol and allow the slides to dry completely at RT.

Create a barrier

1. Draw a barrier 2-4 times around each section with the ImmEdge™ hydrophobic barrier pen (PAP pen).
2. Let the barrier dry completely ~5 min. or overnight at RT.

Load the slides in the RNAscope® EZ-Batch™ Slide Holder

(Instructions in RNAscope® Multiplex Fluorescent Reagent Kit v2 User Manual on page 17.)

Pre-treat 3: Apply RNAscope® Protease Plus

1. Add ~5 drops of RNAscope® Protease Plus to entirely cover each section.
2. Place the RNAscope® EZ-Batch™ Slide Holder in the pre-warmed HybEZ™ Humidity Control Tray. Close the lid, seal, and insert the tray back into the oven.
3. Incubate at 40 °C for 30 min.
    a. Note: If needed, prepare RNAscope® Assay materials during this step.
3. Pour at least 200 ml distilled water into the transparent RNAscope® EZ-Batch™ Wash Tray.
4. Remove the HybEZ™ Humidity Control Tray from the oven. Remove the slide holder from the tray. Place the tray back into the oven.
5. Place the RNAscope® EZ-Batch™ Slide Holder into the wash tray containing water. Make sure all the slides are submerged. Wash the slides 2 X with slight agitation.

Running the RNAscope® assay

1. Prepare probes.
    a. Warm probes for 10 min. at 40 °C in a water bath or incubator, then cool to RT.
    b. Briefly spin the C2/C3/C4 probes to collect the liquid at the bottom of the tubes.

Pipette 1 volume of C2, 1 volume of C3, and 1 volume of C4 probes to 50 volumes of C1 probe (which is ready to use) into a tube. Invert the tube several times to mix.

Hybridize probe

1. Remove excess liquid from the slides while keeping them locked in the RNAscope® EZ-Batch™ Slide Holder. Insert the slide holder into the HybEZ™ Humidity Control Tray.
2. Add 4 drops of the appropriate probe mix to entirely cover each slide.
    a. For example, add four drops of the appropriate probe to a 0,75" x 0,75" barrier.
3. Close the tray and insert into the HybEZ™ Oven for 2 hr at 40 °C.
4. Remove the HybEZ™ Humidity Control Tray from the oven. Remove the slide holder from the tray. Place the tray back into the oven.
5. Wash the slides in 1X Wash Buffer for 2 min. at RT two times.

OPTIONAL STOPPING POINT. You can store the slides in 5X SSC overnight at RT. Before continuing with the assay, wash the slides twice with 1X Wash Buffer for 2 min. at RT.

Equilibrate reagents

1. Remove AMP1, AMP2, AMP3, HRP-C1, HRP-C2, HRP-C3, HRP-C4 and HRP blockers from the refrigerator. Place at RT.
2. Ensure HybEZ™ Oven and prepared Humidity Control Tray are at 40 °C.

Hybridize AMP 1

1. Remove excess liquid from the slides while keeping them locked in the EZ-Batch™ Slide holder. Insert the slide holder into the HybEZ™ Humidity Control Tray.
2. Add 4 drops of RNAscope® Multiplex FL v2 Amp 1 to entirely cover each slide.
3. Close the tray and insert into the HybEZ™ Oven for 30 min. at 40 °C.
4. Remove the HybEZ™ Humidity Control Tray from the oven. Remove the slide holder from the tray. Place the tray back into the oven.
5. Wash the slides in 1X Wash Buffer for 2 min. at RT two times.

Hybridize AMP 2

As AMP1 with RNAscope® Multiplex FL v2 Amp 2.

Hybridize AMP 3

As AMP1 with RNAscope® Multiplex FL v2 Amp 3 except the incubation in oven is 15 min. at 40 °C.

Prepare Opal™ Dye Fluorophores

1. Reconstitute the Opal™ Dyes using the instructions from Perking Elmer.
    a. Reconstitute each Opal™ fluorophores in 75 µl of DMSO.
2. IMPORTANT! Store Opal™ Dye stocks at 2-8 °C. Follow manufacturer's instructions.
3. Determine the volume of Opal™ Dye needed.
4. Dilute the Opal™ Dye using the TSA buffer provided in the RNAscope®.
    a. Start with a 1:1500 dilution.

Develop HRP-C1 signal:

1. Remove excess liquid from the slides while keeping them locked in the EZ-Batch™ Slide holder. Insert the slide holder into the HybEZ™ Humidity Control Tray.
2. Add 4 drops of RNAscope® Multiplex FL v2 HRP-C1 to entirely cover each slide.
3. Close the tray and insert into the HybEZ™ Oven for 15 min. at 40 °C.
4. Place the RNAscope® EZ-Batch™ Slide Holder into the wash tray containing 200 ml 1X Wash Buffer and wash the slides for 2 x 2 min. at RT.
5. Remove excess liquid from the slides and insert the slide holder back into the humidity control tray.
6. Add 150 µl diluted Opal™ 520 to each slide and incubate for 30 min. at 40 °C.
7. Place the RNAscope® EZ-Batch™ Slide Holder into the wash tray containing 200 ml 1X Wash Buffer and wash the slides for 2 x 2 min. at RT. Repeat the wash step with fresh buffer.
8. Remove excess liquid from the slides and insert the slide holder back into the humidity control tray.
9. Add 4 drops of RNAscope® Multiplex FL v2 HRP blocker to entirely cover each slide.
10. Insert the slides into the HybEZ™ Oven for 15 min. at 40°C.
11. Place the RNAscope® EZ-Batch™ Slide Holder into the wash tray containing 200 ml 1X Wash Buffer and wash the slides for 2 x 2 min. at RT.

Develop HRP- C2 signal:

1. As HRP-C1 with HRP-C2 and Opal™ 570.

Develop HRP-C3 signal:

1. As HRP-C1 with HRP-C3 and Opal™ 620.

Develop HRP-C4 signal:

1. As HRP-C1 with HRP-C4 and Opal™ 690.

Counterstain and mount the slides

IMPORTANT! Do this procedure with no more than five slides at a time.

1. Remove excess liquid from slides and add ~4 drops of DAPI to each slide.
2. Incubate for 30 seconds at RT.
3. Remove DAPI by tapping or flicking the slides, and immediately place 1-2 drops of ProLong™ Gold Antifade Mountant on each slide.
4. Carefully place a 24 mm x 50 mm glass coverslip over the tissue section. Avoid trapping air bubbles.
5. Dry slides 30 min. to overnight in the dark.
6. Store slides in the dark at 2-8 °C.

2. Vector® TrueVIEW™ Autofluorescence Quenching Kit, Cat. No.: SP-8400 (modified after Vector Laboratories)

Kit components

Product name and volume:

Vector TrueVIEW™ Reagent A, 5 ml

Vector TrueVIEW™ Reagent B, 5 ml

Vector TrueVIEW™ Reagent C, 5 ml

VECTASHIELD® Vibrance™ Antifade Mounting Medium, 2 ml

Storage

- Store reagents in original bottles at 2-8 °C.
- Avoid storing reagents or working solution in strong direct light.

Important assay optimization process:

1) Determine the extent of autofluorescence with NEGATIVE CONTROL unstained sections (i.e., no detection reagents).
2) On adjacent NEGATIVE control unstained sections, observe the quenching effect of the TrueVIEW™ reagent with 2-5 min. incubation.
3) After establishing the control parameters described in 1 & 2 above, optimize the primary antibody dilution to achieve desired signal to noise ratio when using TrueVIEW™ quenching solution.
4) The mounting medium has a significant impact on the performance of this product. Substitution with a different mounting medium, other than what is provided in the kit, may dramatically affect the outcome. Vector TrueVIEW™ quenching reagent has been optimized for use with VECTASHIELD® Vibrance™ (included in the kit) and this combination is highly recommended to achieve the best results.

Instructions for use:

A) Reagent Preparation

For each standard tissue section in your assay, you will need approximately 150 µl of Vector TrueVIEW™ Reagent (i.e., 50 µl A + 50 µl B + 50 µl C). To prepare Vector TrueVIEW™ Reagent, a ratio of 1:1:1 of Reagents A, B and C is required. The order of mixing is important.

1. Add equal volumes of Reagent A and Reagent B in a clean test tube. Mix for 10 seconds.
2. Add Reagent C to the mixture (ensuring a 1:1:1 volume ratio) and mix again for 10 seconds.

Vector TrueVIEW™ Reagent is now ready to use. Once prepared, Vector TrueVIEW™ Reagent is stable for at least 2 hours at RT.

B) Tissue Treatment Procedure

Following completion of the immunofluorescent staining:

1. Drain excess buffer from tissue section.
2. Add Vector TrueVIEW™ Reagent to cover tissue section completely (~150 µl); and incubate for 2-5 min.
3. Wash in PBS buffer for 5 min.
4. Drain excess buffer from section. Optimal results are obtained if excess buffer is removed around tissue prior to adding mounting medium.
5. Dispense VECTASHIELD® Vibrance ™Antifade Mounting Medium onto the tissue section. Coverslip and allow VECTASHIELD® Vibrance™ Antifade Mounting Medium to disperse over the entire section.
6. Slides can be visualized immediately after mounting, but the coverslip will not be immobilized until mounting media is cured at RT for 1-2 hours.
7. For optimal results, slides should be evaluated within 48 hours of mounting.

C) Nuclear Counterstaining

Nuclear counterstaining can be performed after TrueVIEW™ treatment. Counterstain concentration may need to be increased to achieve optimal signal to noise. For DAPI staining, we recommend using DAPI at 5 µg/ml in PBS buffer for 10 min, and then mounting with the included VECTASHIELD® Vibrance™ Antifade Mounting Medium.

3. Immunofluorescence staining protocol, 1st

1. Paraffin removal.
    a) Xylene 3 x 5 min.
    b) EtOH 100 % 2 x 3 min.
    c) EtOH 95 % 2 x 3 min.
    d) EtOH 70 % 2 x 3 min.
    e) dH_2O 5 min.
    f) PBS 5 min.
2. Antigen retrieval with 10 mM Citrate buffer pH 6,0.
    a) Add 750 ml of MilliQ H_2O to the pressure cooker.
    b) Put samples in the cooker bucket.
    c) Immerse samples in citrate buffer (fill bucket).
    d) Set the pressure cooker to start (it will take only 20 min, but you can open the cooker after 2 h).
    e) After 2 h, take the bucket and let the citrate buffer cool at RT.
    f) Wash the slides in PBS at RT 2 X 5min.
3. Circle sections with grease pen.
4. Block samples with 5 % NGS + 3 % BSA in PBS for 1 h at RT.
5. Remove blocking solution (from all samples except the secondary antibody control).
6. Add diluted primary and conjugated antibodies: dilute in blocking solution (5 % NGS + 3 % BSA in PBS) and incubate in dark humified chamber at +4 °C overnight.
7. Wash with PBS 3 x 5 min.
8. Incubate with secondary antibody for 1 h at RT diluted in 10 % NGS + 5 % BSA.
9. Wash in 0,1% Triton X-PBS 3 x 5 min. (slides into solution).
10. Mount with ProLong™ Gold Antifade reagent with DAPI.
11. Let the slides dry in dark for 24 h before imaging.

4. Immunofluorescence staining protocol, 2nd

1. Paraffin removal (same as in Appendix 3).
2. Antigen retrieval with 10 mM Citrate buffer pH 6,0.
    a) Place the slides into a plastic jar, do not cover the jar and put it in a microwave.
    b) Switch on the microwave to 300 W for 8 minutes (4 min. on + 30 sec. rest + 4 min. on), let the jar cool down for 2 minutes and put it in the microwave for 7 minutes (3,5 min. on + 30 sec. rest + 3,5 min. on).
    c) After cooling down to RT for at least 15 min. wash slides 4 x 3 min. in milliQ H_2O.
    d) Wash the slides in PBS at RT 3 x 5min.
3. Circle sections with a grease pen.
4. Block samples with 5 % NGS + 3 % BSA in PBS-T (PBS + 0,05 % Tween-20) for 1 h at RT.
5. Remove blocking solution (from all samples except the secondary antibody control).
6. Add diluted primary: dilute in blocking solution (5 % NGS + 3 % BSA in PBST) and incubate in dark humified chamber overnight at +4 °C.
7. Wash with PBS-T 3 x 5 min.
8. Add secondary antibodies diluted in blocking solution. Incubate 1 h at 37 °C.
9. Wash in PBS-T 3 x 5 min. (slides into the solution).
10. Mount with ProLong™ Gold Antifade reagent with DAPI.

Let the slides dry in dark for 24 h before imaging.

5. Haematoxylin & eosin staining protocol

Preparations:

- Make sure that rehydration and dehydration alcohol series are filled up and first xylene is clean enough.
- Filter dyes through Whatmann paper.
- Let slides to cool down or warm up to RT before rehydration.

Staining protocol:

1. Deparaffinization and rehydration:
    a. Xylene 3 x 5 min. (shake off loose xylene from slides before proceeding to ethanol series).
    b. 100 % EtOH 3 x 2 min.
    c. 96 % EtOH 2 x 2 min.
    d. 70 % EtOH 2 x 2 min.
    e. 50 % EtOH 2 min.
    f. dH_2O 5 min. (shake off loose water from slides before proceeding to haematoxylin).
2. Place in Mayer's haematoxylin (Sigma MHS16) for 15 min.
3. Rinse in warm running tap water for 15 min.
4. Rinse in dH_2O for 30 seconds.
5. Rinse in 96 % EtOH for 30 seconds (shake off loose ethanol from slides before proceeding to eosin).
6. Place in Eosin (Sigma HT110116) for 45 seconds.
7. Dehydration:
    a. 96 % EtOH 1 min.
    b. 100 % EtOH 3 x 1 min.
    c. Xylene 2 x 5 min.
8. Mount with DPX mountant for histology (Sigma 06522) and leave slides to dry in fume hood for 2-3 days.

6. Positive and negative control images from the RNAscope® staining experiments

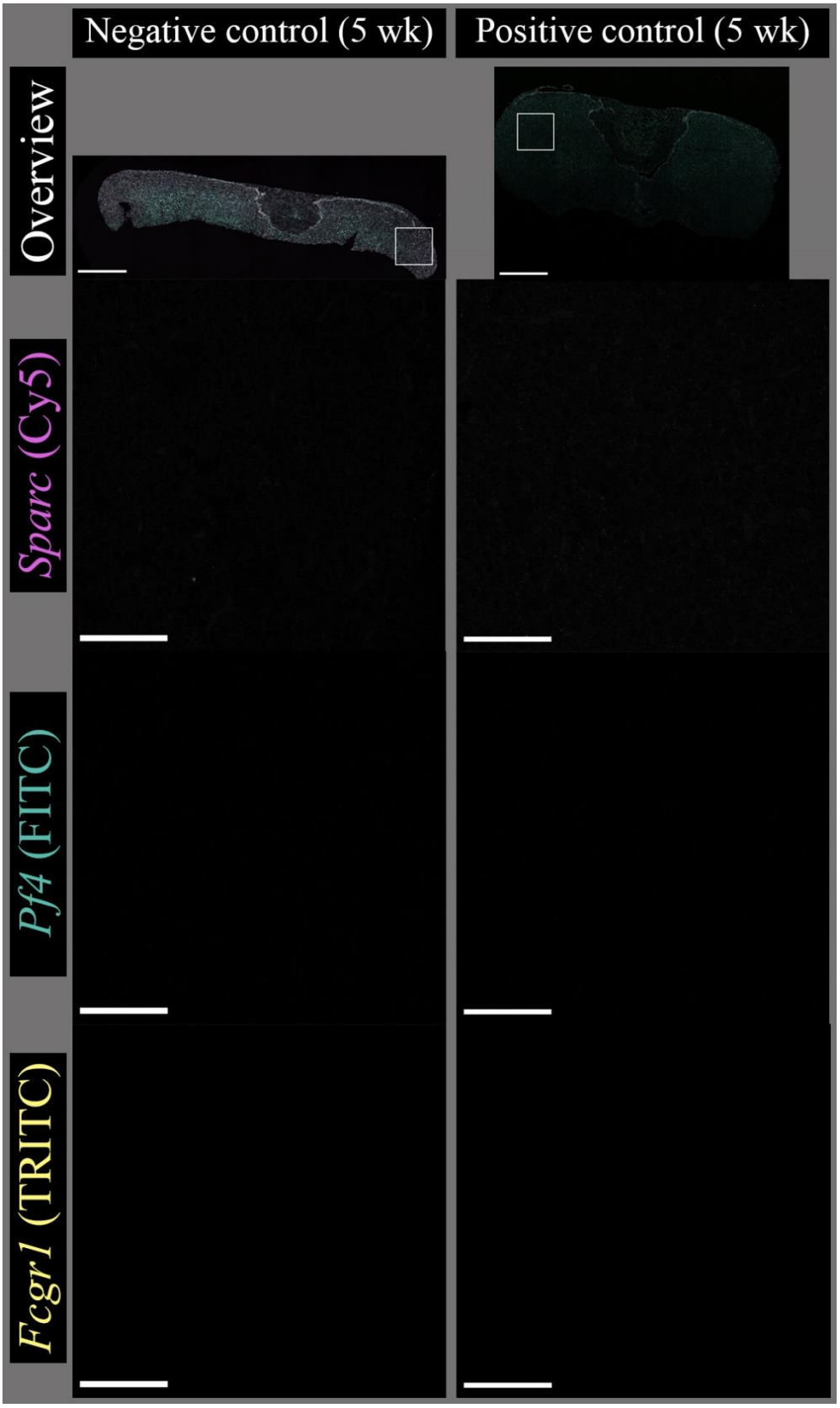

A. Control pituitary sections (1st staining experiment) from 5-week-old C57BL/6NRj mice. Scale bars in the overview images are 400 µm and in the close-ups, from the regions of interest, 50 µm. The target signal colours in the overview images are the same as the colours in target/channel names. Nuclei are shown in the overview images in grayscale.

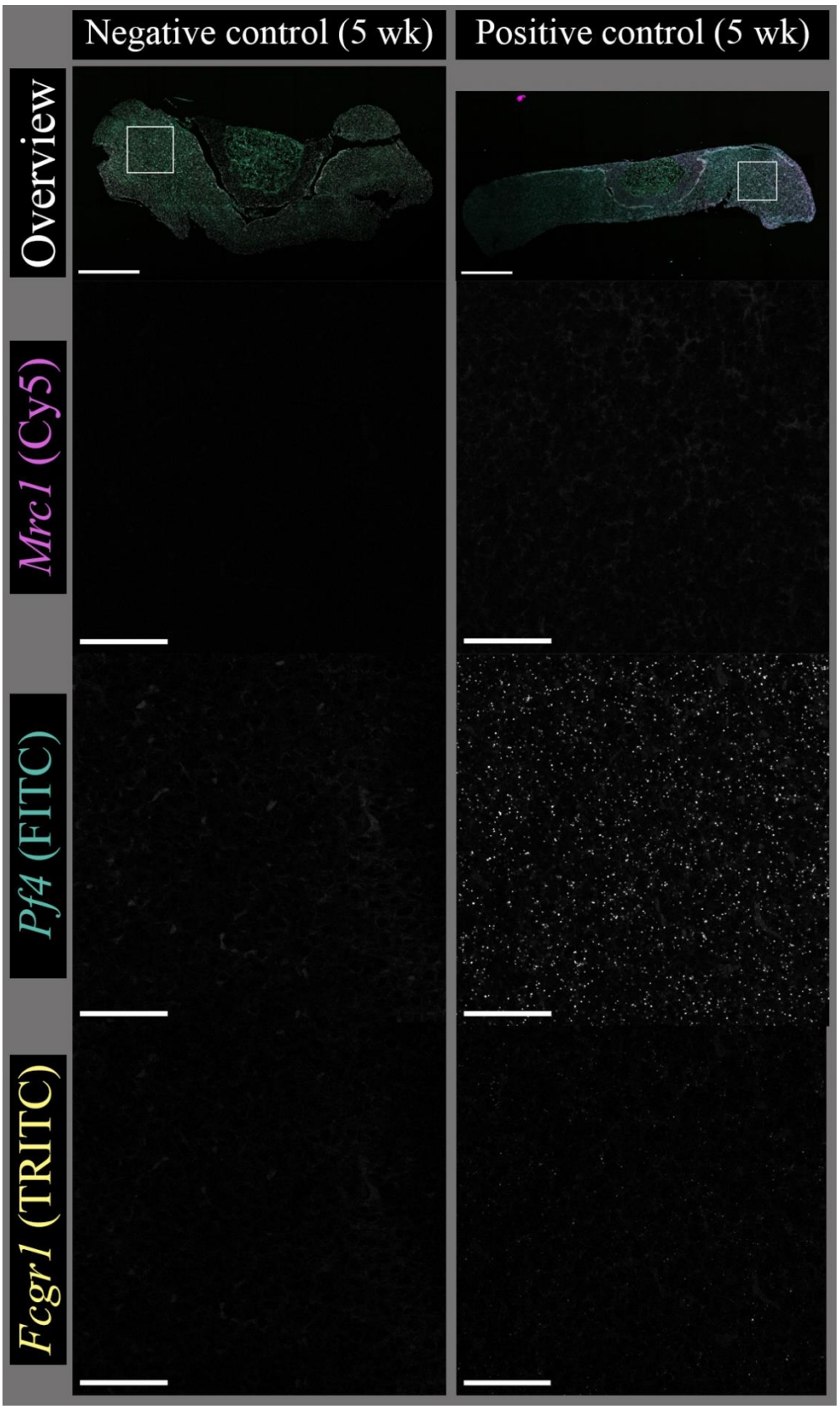

B. Control pituitary sections (2nd staining experiment) from 5-week-old C57BL/6NRj mice. Scale bars in the overview images are 400 µm and in the close-ups, from the regions of interest, 50 µm. The target signal colours in the overview images are the same as the colours in target/channel names. Nuclei are shown in the overview images in grayscale.

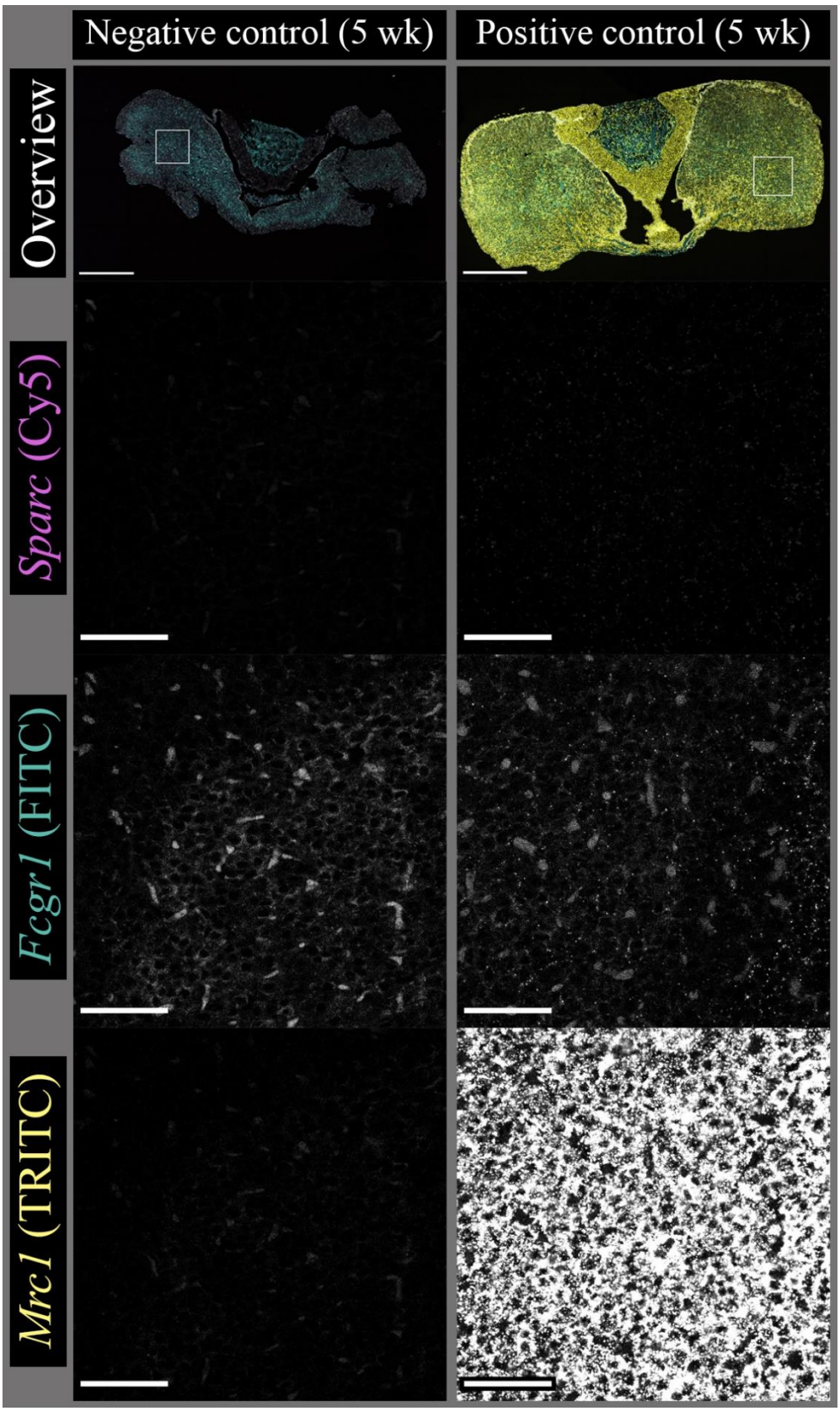

C. Control pituitary sections (3rd staining experiment) from 5-week-old C57BL/6NRj mice. Scale bars in the overview images are 400 µm and in the close-ups, from the regions of interest, 50 µm. The target signal colours in the overview images are the same as the colours in target/channel names. Nuclei are shown in the overview images in grayscale.